Monthly Notices of the ROYAL ASTRONOMICAL SOCIETY

MNRAS **512,** 3079–3097 (2022) https://doi.org/10.1093/mnras/stac622
Advance Access publication 2022 March 9

# Stellar masses of clumps in gas-rich, turbulent disc galaxies

Liyualem Ambachew [1,2]★ Deanne B. Fisher [1,2] Karl Glazebrook,[1,2] Marianne Girard [1,2] Danail Obreschkow [2,3] Roberto Abraham,[4] Alberto Bolatto,[5,6,7] Laura Lenkić [5,8] and Ivana Damjanov[9]

[1]*Centre for Astrophysics and Supercomputing, Swinburne University of Technology, PO Box 218, Hawthorn, VIC 3122, Australia*
[2]*ARC Centre of Excellence for All Sky Astrophysics in 3 Dimensions (ASTRO 3D), Australia*
[3]*International Centre for Radio Astronomy Research (ICRAR), M468, University of Western Australia, 35 Stirling Hwy., Crawley, WA 6009, Australia*
[4]*Department of Astronomy & Astrophysics, University of Toronto, 50 St. George St., Toronto, ON M5S 3H8, Canada*
[5]*Department of Astronomy, University of Maryland, College Park, MD 20742, USA*
[6]*Visiting Scholar, the Flatiron Institute, Center for Computational Astrophysics, NY 10010, USA*
[7]*Visiting Astronomer, National Radio Astronomy Observatory, VA 22903, USA*
[8]*SOFIA Science Center, USRA, NASA Ames Research Center, M.S. N232-12, Moffett Field, CA 94035, USA*
[9]*Department of Astronomy & Physics, Saint Mary's University, 923 Robie St, NS B3H 3C3, Canada*

Accepted 2022 March 2. Received 2022 March 2; in original form 2021 October 22

## ABSTRACT

In this paper, we use *Hubble Space Telescope*/WFC3 observations of six galaxies from the DYnamics of Newly Assembled Massive Object (DYNAMO) survey, combined with stellar population modelling of the SED, to determine the stellar masses of DYNAMO clumps. The DYNAMO sample has been shown to have properties similar to $z \approx 1.5$ turbulent, clumpy discs. DYNAMO sample clump masses offer a useful comparison for studies of $z > 1$ in that the galaxies have the same properties, yet the observational biases are significantly different. Using DYNAMO, we can more easily probe rest-frame near-IR wavelengths and also probe finer spatial scales. We find that the stellar mass of DYNAMO clumps is typically $10^7-10^8 M_\odot$. We employ a technique that makes non-parametric corrections in removal of light from nearby clumps, and carries out a locally determined disc subtraction. The process of disc subtraction is the dominant effect, and can alter clump masses at the 0.3 dex level. Using these masses, we investigate the stellar mass function (MF) of clumps in DYNAMO galaxies. DYNAMO stellar MFs follow a declining power law with slope $\alpha \approx -1.4$, which is slightly shallower than, but similar to what is observed in $z > 1$ lensed galaxies. We compare DYNAMO clump masses to results of simulations. The masses and galactocentric position of clumps in DYNAMO galaxies are more similar to long-lived clumps in simulations. Similar to recent DYNAMO results on the stellar population gradients, these results are consistent with simulations that do not employ strong 'early' radiative feedback prescriptions.

**Key words:** galaxies: evolution – galaxies: formation – galaxies: star formation.

## 1 INTRODUCTION

Most of the stars in the Universe are formed at $z \sim 2$ (e.g. Hopkins & Beacom 2006; Madau & Dickinson 2014). The first Hubble Deep Field surveys revealed that the highly star-forming galaxies at this epoch have irregular morphologies compared to local Hubble Sequence galaxies and are dominated by a few bright patches (Abraham et al. 1996). When these bright patches are viewed edge-on, they appear in lines, and thus often referred to as 'chain galaxies' (Cowie 1995). The appearance of these star-forming galaxies suggests that these bright knots are embedded in disc-like systems. Follow-up studies showed that they represent massive clusters of young stars with sizes of an $\sim$ kpc (e.g. Elmegreen & Elmegreen 2005). These giant clumps are detected in the deep and high-resolution rest-frame UV (e.g. Elmegreen & Elmegreen 2005; Schreiber et al. 2009), as well as in the rest rest-frame optical-line emissions (e.g. Jones et al. 2010; Genzel et al. 2011; Livermore et al. 2012, 2015; Fisher et al. 2017a).

Early explanations of origin of clumps focused primarily on major mergers (e.g. Conselice et al. 2003). However, later kinematic studies of star-forming galaxies at redshift $z \sim 2$ (Genzel et al. 2006; Shapiro et al. 2008; Schreiber et al. 2009) revealed that a significant fraction of clumpy galaxies do not show ongoing merger signatures. Rather the galaxies have rotating velocity fields in spite of their clumpy morphology.

A popular theory for clump formation, currently, is via self-gravitating instabilities (e.g. Noguchi 1999; Bournaud, Elmegreen & Elmegreen 2007; Elmegreen, Bournaud & Elmegreen 2008; Dekel, Sari & Ceverino 2009; Ceverino, Dekel & Bournaud 2010). The scenario of clumps being formed through violent gravitational instabilities is supported by some observational studies such as Bournaud et al. (2007); Genzel et al. (2011); Guo et al. (2012); Fisher et al. (2017a); and White et al. (2017). Alternate evidence of clump formation through self-gravitating disc is found in their stellar mass function (MF). If clumps form internally, their resulting stellar

★ E-mail: ltilahun@swin.edu.au

MF would follow a declining power law with a slope of $\sim -2$ (e.g. Dessauges-Zavadsky & Adamo 2018). The recent VELA simulation study by Huertas-Company et al. (2020) finds that slope of the clump stellar MF can be $\sim -1.5$. Alternate theories for how clumps form in discs have been put forward, including through spiral arm instabilities (Inoue & Yoshida 2018) or bottom up collisions of smaller clumps (Behrendt, Burkert & Schartmann 2016). While it is likely that many clumpy galaxies at $z > 1$ are indeed the result of merging, it is none the less commonly accepted that some disc processes are generating large star-forming complexes within gas-rich discs.

Estimating the lifetime of clumps remains a one of the main goals in this field, for multiple reasons. First, it is important to understand the ultimate fate of clumps, and if they contribute to bulges in local Universe. Secondly, a wealth of simulation work suggests that the details of feedback prescriptions have a significant impact on lifetime, and therefore current stellar mass of clumps (Hopkins et al. 2012; Mandelker et al. 2016; Mayer et al. 2016). To first order, this can be understood in that clumps have star formation rate (SFR) surface densities that are orders-of-magnitude higher than what is observed in local spirals; subtle changes to stellar feedback models can have amplified affects in inside clumps.

Estimating the longevity of clumps, however, is not a simple task. Lenkić et al. (2021) show, also with DYNAMO galaxies, that individual clumps do not have a single age, but gradients in colour profiles indicate a growing system. These results imply that using a single age for clumps, derived from stellar populations will be biased toward younger ages than the true age of clumps. The simulations of Bournaud et al. (2014) show that clumps can continue to accrete gas for new star formation, rendering the light-weighted stellar population a poor metric of the clump lifetime, as it may always be young. Lenkić et al. (2021) find that using the maximum age found in clumps improves clump age-galactocentric distance correlations, and may indicate a long-lived system.

A significant body of work suggests that resolution and sensitivity are critical for measuring the properties of clumps, including their stellar mass. *HST* observations of unlensed galaxies suggest that stellar masses of clumps are roughly $10^8 - 10^9$ $M_\odot$ (e.g. Schreiber et al. 2011; Guo et al. 2012). However, studies of gravitational lensed high-$z$ systems find a characteristic clump luminosity that is lower than in unlensed studies high-$z$ galaxies (e.g. Jones et al. 2010; Livermore et al. 2012; Cava et al. 2017; Dessauges-Zavadsky et al. 2017). Dessauges-Zavadsky et al. (2017) compare stellar masses of clumpy star-forming galaxies at redshift of $1.1 < z < 3.6$ in lensed or unlensed galaxies. They argue that the systematic uncertainties due to spatial resolution and sensitivity significantly affect the selection and measurement of clump properties, which cause the resulting clump stellar mass distribution to be biased toward higher masses. Moreover, Cava et al. (2017) analysed multiple images of the same gravitationally lensed galaxy at different magnification, finding that unlensed observations with $\sim$1 kpc resolution tend to overestimate both the size and luminosity of clumps, and therefore the mass. A particular problem with unlensed studies of clumps is the blending of smaller clumps into a single resolution element. Fisher et al. (2017a) show in more detail how the clustering of smaller clumps when imaged at $\sim$1 kpc resolution results in clump properties similar to those in unlensed $z \sim 2$. They find that fluxes and sizes are significantly impacted when images are blurred. In addition to observational studies, simulation results also show that 100 pc resolution is needed to isolate clumps (Tamburello et al. 2017).

In this paper, we use a sample of local galaxies called DYnamics of Newly Assembled Massive Object (DYNAMO; Green et al. 2014). The DYNAMO sample was selected from the Sloan Digital Sky Survey to be the brightest H$\alpha$ emitting galaxies that do not contain AGNs. DYNAMO galaxies have properties that are similar to those of star-forming $z \sim 2$ galaxies, but yet are located at $z \sim 0.1$ (e.g. Bassett et al. 2014; Green et al. 2014; Fisher et al. 2014, 2019; Oliva-Altamirano et al. 2017; White et al. 2017; Girard et al. 2021). Therefore, they can be observed with significantly improved spatial resolution and deeper sensitivity, and allow us to measure clump properties with greater precision addressing the biases discussed above.

In this work, we will use results from *HST* observations, combined with stellar population modelling of the spectral energy distribution (SED), to estimate the masses of individual clumps in DYNAMO galaxies. Our results allow for a controlled comparison of clumps with improved spatial resolution and wavelength coverage for comparison to results of large surveys of $z \sim 2$ observations with *Hubble Space Telescope* (*HST*) and in the near future James Webb Space Telescope (JWST).

## 2 THE DATA AND SAMPLE

### 2.1 Sample

For this work, we used a subset of six galaxies from the DYNAMO sample. The full DYNAMO sample is described in detail in Green et al. (2014). DYNAMO galaxies were selected from Sloan Digital Sky Survey (SDSS) DR4 (Adelman-McCarthy et al. 2006), excluding galaxies with AGNs. DYNAMO galaxies are found in the local Universe within redshift range of $z = 0.075 - 0.13$ that have a high SFR. The full DYNAMO sample was then observed with integral field spectroscopy observations of H$\alpha$.

In this study, we use a subset of more well-studied galaxies from DYNAMO. The key feature of the follow-up DYNAMO sub-sample is that a kinematic selection was made from the original DYNAMO survey (Green et al. 2014). The DYNAMO team identified a sub-sample of galaxies with rotating kinematics and high-velocity dispersion in the seeing limited observations. Those galaxies were then rigorously tested to confirm their similarity to $z \approx 1-2$ galaxies. After those test, we have then concentrated on those targets, which more robustly match the observations of distant galaxies.

Several studies show similarities between DYNAMO galaxy properties and $z \sim 1.5$ star-forming galaxies.To investigate the morphological similarity between DYNAMO and z $\sim$ 2 galaxies, Fisher et al. (2017a) degrade the resolution of *HST* H$\alpha$ maps of DYNAMO galaxies to the physical resolution of $z \sim 2$ galaxies. They found, at matched resolution, that the clumps in DYNAMO galaxies are as bright as and have similar diameters to $z \sim 2$ galaxies. Clumps in DYNAMO galaxies also meet the definition of clumpy galaxies as defined by the CANDELS results (Guo et al. 2015). DYNAMO galaxies have high internal gas velocity dispersions, $\sigma \approx 20-100$ km s$^{-1}$ (Green et al. (Bassett et al. 2014; Green et al. 2014; Oliva-Altamirano et al. 2017; Girard et al. 2021). They also have lower angular momentum for their stellar mass (Obreschkow et al. 2015), which is consistent with $z \sim 2$ star-forming galaxies with similar mass (Swinbank et al. 2017). Galaxies at $z \sim 1-2$ have been shown to have gas fractions of $f_{\rm gas} \sim 20-80$ per cent (Tacconi et al. 2013). However, local spirals have gas fractions roughly $\sim 1-5$ per cent (Saintonge et al. 2012). DYNAMO galaxies have been shown to have high fractions of molecular gas, $M_{\rm gas}/M_{\rm tot} \approx 10-70$ per cent, $f_{\rm gas}$ like $z \sim 2$ galaxies (Fisher et al. 2014, 2019; White et al. 2017); and have large clumps in both H$\alpha$ gas and rest-frame *UV* starlight that are consistent with large clumps of star formation similar to what is observed at $z > 1$ (Fisher et al. 2017a;

**Table 1.** Properties of six DYNAMO – *HST* Targets.

| Galaxy | $z$ | RA | Dec. | SFR[a] ($M_\odot\ yr^{-1}$) | $M_*^a$ ($10^{10}\ M_\odot$) | $f_{gas}^b$ | $\sigma^b$ ($km\ s^{-1}$) | $V_{flat}^b$ ($km\ s^{-1}$) | $A_{H_\alpha}{}^c$ (mag) |
|---|---|---|---|---|---|---|---|---|---|
| G04-1 | 0.1298 | 04:12:19.7100 | –05:54:48.60 | 41.6 ± 2.2 | 6.45 | 0.33 ± 0.04 | 50 | 269 | 1.52 ± 0.26 |
| G14-1 | 0.1323 | 14:54:28.3300 | +00:44:34.30 | 8.3 ± 0.9 | 2.23 | 0.77 ± 0.08 | 70 | 136 | – |
| G08-5 | 0.1322 | 08:54:18.7300 | +06:46:20.60 | 16.6 ± 1.0 | 1.73 | 0.30 ± 0.05 | 64 | 243 | – |
| G20-2 | 0.1411 | 20:44:2.9150 | –06:46:57.90 | 17.3 ± 0.7 | 2.16 | 0.21 ± 0.05 | 81 | 166 | 0.89 ± 0.1 |
| D13-5 | 0.0753 | 13:30:07.009 | 00:31:53.450 | 21.2 ± 0.9 | 5.38 | 0.36 ± 0.02 | 46 | 192 | 1.80 ± 0.52 |
| D15-3 | 0.0671 | 15:34:35.3900 | –00:28:44.50 | 13.7 ± 1.0 | 5.42 | 0.17 ± 0.04 | 45 | 240 | – |

*Notes*.[a]Values from Green et al. (2014).
[b]Values from Fisher et al. (2017a; 2019).
[c]H$\alpha$ extinction from Bassett et al. (2017).

Lenkić et al. 2021). In the most recent DYNAMO study, Lenkić et al. (2021) show that these clumps are not likely the result of 'holes' in extinction profiles, but are structures of stars. This has also been shown by Elmegreen & Elmegreen (2005) in $z \sim 2$ galaxies, where they find clumps have high average density $\sim 0.2\ M_\odot\ pc^{-3}$.

A key issue with studies of highly star-forming galaxies in the local Universe is identifying merging galaxies. For DYNAMO, we use three indicators associated to merging. First, we observe kinematics with higher spatial (0.15-0.7 arcsec) resolution (Bassett et al. 2014; Oliva-Altamirano et al. 2017), second we observe dust temperatures (White et al. 2017); and finally we use *HST*-based high spatial resolution maps of *HST* H$\alpha$ and 600-nm continuum (Fisher et al. 2017a). We only selected systems that are not consistent with merging, as indicated by order rotation in higher spatial resolution ionized gas velocity maps, lower dust temperatures ($T_{dust} \sim 20-30$ K) and exponentially decaying stellar surface brightness profile (Fisher et al. 2017a).

Generally, the properties of DYNAMO galaxies resemble galaxies at $z \sim 2$. DYNAMO galaxies are therefore used as laboratories for studying the processes in clumpy, turbulent discs with higher resolution and sensitivity. Our sample properties span stellar mass $(1.7-6.4) \times 10^{10}\ M_\odot$, SFR $\sim 6.9-21\ M_\odot\ yr^{-1}$, and extinction A(H$\alpha$) $\sim$0.59−1.27 mag. The properties of these six DYNAMO galaxies are listed in Table 1.

### 2.2 DYNAMO galaxies as clumpy disc

A number of works in the literature establish the similarity of DYNAMO galaxies to turbulent, gas-rich disc galaxies, more commonly observed at $z \sim 1-3$ (e.g Bassett et al. 2014; Green et al. 2014; Fisher et al. 2014; Obreschkow et al. 2015; Bassett et al. 2017; Oliva-Altamirano et al. 2017; White et al. 2017; Fisher et al. 2017a, 2017b, 2019; Girard et al. 2021; Lenkić et al. 2021). Green et al. (2014) show that in the overall sample, ∼84 per cent of DYNAMO galaxies have disc-like light profiles and ∼ 50 per cent are located on the Tully–Fisher relation (Green et al. 2014). Follow-up observations of DYNAMO galaxies were made a sample down selected to be more consistent with having rotating disc kinematics, high SFR, and high H$\alpha$ velocity dispersion. Bassett et al. (2014) used deep Gemini/GMOS observations to show that DYNAMO galaxies are rotating in both stars and gas. Oliva-Altamirano et al. (2017) used Keck adaptive optics observations to show that the observation of rotation is not an artefact of poor resolution, but still holds with resolution of ∼150 pc. Fisher et al. (2017b) found that from 10 DYNAMO galaxies, 8 (6 are analyzed in this work) of them have disc-like exponential decaying surface brightness profile using *HST* 600 nm continuum maps. Fisher et al. (2017b) show using *HST* images that the H$\alpha$ emission is 'clumpy'. They find that when you degrade the DYNAMO images to match the same physical resolution and sensitivity as found in AO images of $z \approx 1.5$ galaxies that the distribution of sizes and luminosity of detected clumps is similar to those in high-$z$ samples (e.g. Genzel et al. 2011; Guo et al. 2015). Both Fisher et al. (2017a) and White et al. (2017) show that the gas densities and kinematics of DYNAMO discs are consitent with marginal stability, i.e. $Q \approx 1$. This is consistent with standard expectations of high-$z$ discs.

There are several papers outlining the star formation and gas properties of DYNAMO galaxies. A key difference from local galaxies is the gas fraction. DYNAMO galaxies have $f_{gas} \approx 0.15-0.6$ (Fisher et al. 2014; White et al. 2017; Fisher et al. 2019; Girard et al. 2021), which is similar to $z \approx 1.5$ galaxies, and makes them 99th percentile outliers from samples of local rotating galaxies of similar mass (Saintonge et al. 2012; Tacconi et al. 2018). The dust in DYNAMO galaxies is found to have low dust temperatures, $T_{dust} \approx 20-30$ K (White et al. 2017), which is dissimilar from local Universe galaxies of the same infrared luminosity. The low dust temperature implies the geometry of the gas and dust is more like that of thick-discs, as in $z \sim 1-2$ galaxies. Similarly, work in progress (Lenkić et al., in preparation) finds that the CO line ratios are similar to those of BzK galaxies (Daddi et al. 2015). Fisher et al. (2019) report the depletion time of DYNAMO galaxies to be anticorrelated with the gas velocity dispersion. The clumpy, high-velocity dispersion DYNAMO galaxies have depletion times of order $t_{dep} \approx 0.3-1.0$ Gyr, which is similar to observations of $z \approx 1.5$ main-sequence galaxies (Tacconi et al. 2018). Systems with less prominent clumps and lower velocity dispersion (e.g. D15-3 in this work) have $t_{dep} \approx 1-2$ Gyr. The DYNAMO team is currently working on producing a kiloparsec-scale resolved Kennicutt–Schmidt analysis, which includes galaxies from this sample. DYNAMO galaxies are found to have high molecular gas surface densities ($\Sigma_{mol} \approx 10^2-10^3\ M_\odot\ pc^{-2}$). We refer the reader to Lenkić et al. (in preparation) for those results, see also the recent work of Fisher et al. (2022).

The origin of DYNAMO galaxies remains a mystery. The gas fractions of DYNAMO galaxies imply that they must have recently undergone an event that mimicked a gas-rich accretion event. However, simply having large gas reservoirs is not sufficient to lead to clumpy star formation and turbulent kinematics. Catinella & Cortese (2015) find a sample of very gas-rich discs at similar redshift; these discs are selected for HI brightness and are not compact like DYNAMO. They do not find high gas velocity dispersions, nor clumpiness (Cortese, Catinella & Janowiecki 2017). The DYNAMO team is currently working to estimate the total gas reservoir of DYNAMO galaxies (Obreschkow et al., in preparation). One observation that is particularly informative is that they are low angular momentum systems. Obreschkow et al. (2015) compare DYNAMO galaxies to the location in the $j_*-M_*$ diagram. DYNAMO galaxies– despite

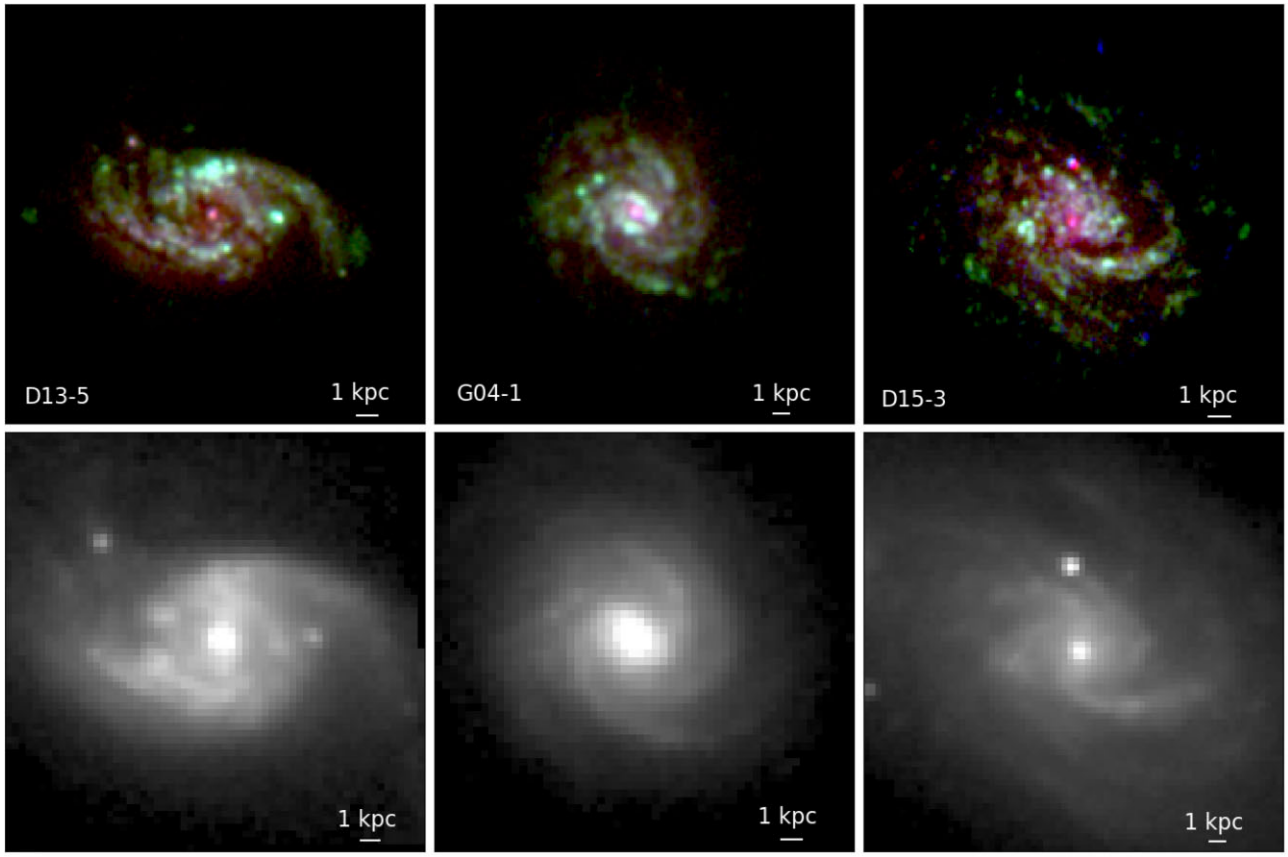


**Figure 1.** Three colour images of DYNAMO galaxies D13-5, G04-1, and D15-3 created using *F336W*, *F467M*, and *FR647M* filters at ∼0.05-arcsec resolution (top row). Bottom row shows the same galaxies observed at ∼0.13-arcsec resolution in the *F125W* filter. The white line in the bottom right-hand corner of each image corresponds to 1 kpc. Though clumps are less prominent in the *F125W* image, we do still see large knots of emission.

being rotating, exponential discs – are found to have low angular momentum, more similar to galaxies at $z \approx 1-2$ (Swinbank et al. 2017; Espejo Salcedo et al. 2022). The implication is that in order to be a clumpy galaxy both large gas accretion and low angular momentum are necessary.

### 2.3 DYNAMO *HST* observation

Observations of our six DYNAMO galaxies were taken during the *HST* Cycle 25 program (Proposal ID 15069, PI: D.B.Fisher) using WFC3 UVIS and IR modes. These observations were performed using UV band-pass (*F225W*), optical band-passes (*F336W*, *F467M*) and near-IR band-pass (*F125W*) filters, as well as *FR647M* filter from an ACS/WFC Cycle 20 program (Proposal ID 12977, PI: I. Damjanov).

Our data set covers a wavelength range from near-UV to near-IR. This is intended to reduce well-known degeneracies between mass-to-light ratio, extinction, and metallicity (Bell & de Jong 2001). Our principle aim is to use SED-fitting techniques to measure the stellar mass and mass-to-light ratio in sub-kpc regions in clumpy galaxies. Taylor et al. (2011) show that of the stellar population parameters derived from SED fitting, mass-to-light ratio is relatively robust, with more significant degeneracies occurring among other parameters (e.g. age, extinction, metallicity). Previous studies show that using optical-plus-near-IR data significantly increases the ability to derive robust mass-to-light ratios from SED-fitting methods (e.g. Bell & de Jong 2001; Zibetti, Charlot & Rix 2009). This principle motivates our choice of five filters ranging from rest-frame ∼200 to ∼1100 nm. In comparison to samples of galaxies at $z > 1$, the DYNAMO sample is the only set of clumpy disc galaxies in which rest-frame near-IR observations are possible. We directly assess the effect that the inclusion of near-IR data set has on the derived clump stellar mass for our DYNAMO sample in Section 3.4 and Fig. 8.

We also have chosen optical filters to avoid strong emission lines (e.g. H$\beta$, [OIII] 5007, and H$\alpha$) in our target galaxies. We present *HST* composite image created from *F336W*, *F467M*, and *FR647M* filters and single-filter *F125W* images Figs 1 and 2. The top panel shows composit RGB image and the bottom panel shows the same galaxies in *F125W* filters. All images were reduced using the standard *HST* pipeline and combined with DRIZZLE.

## 3 METHODS

In the following subsections, we give detailed descriptions of each step in our process. First, we give a general overview.

In order to measure the masses of individual clumps, we must first locate clumps, then we used SED-fitting code to measure the clump stellar mass. Clump positions are located in the *F336W* images, which is similar to clump position selection in $z \approx 1-3$ *HST* surveys (e.g. Guo et al. 2015).

The spatial resolution of the WFC3/IR instrument used to measure the *F125W* band images is 0.13 arcsec per pixel. This resolution is more than a factor of 2 times larger than the resolution of WFC3/UVIS and ACS/WFC images that cover the optical light.

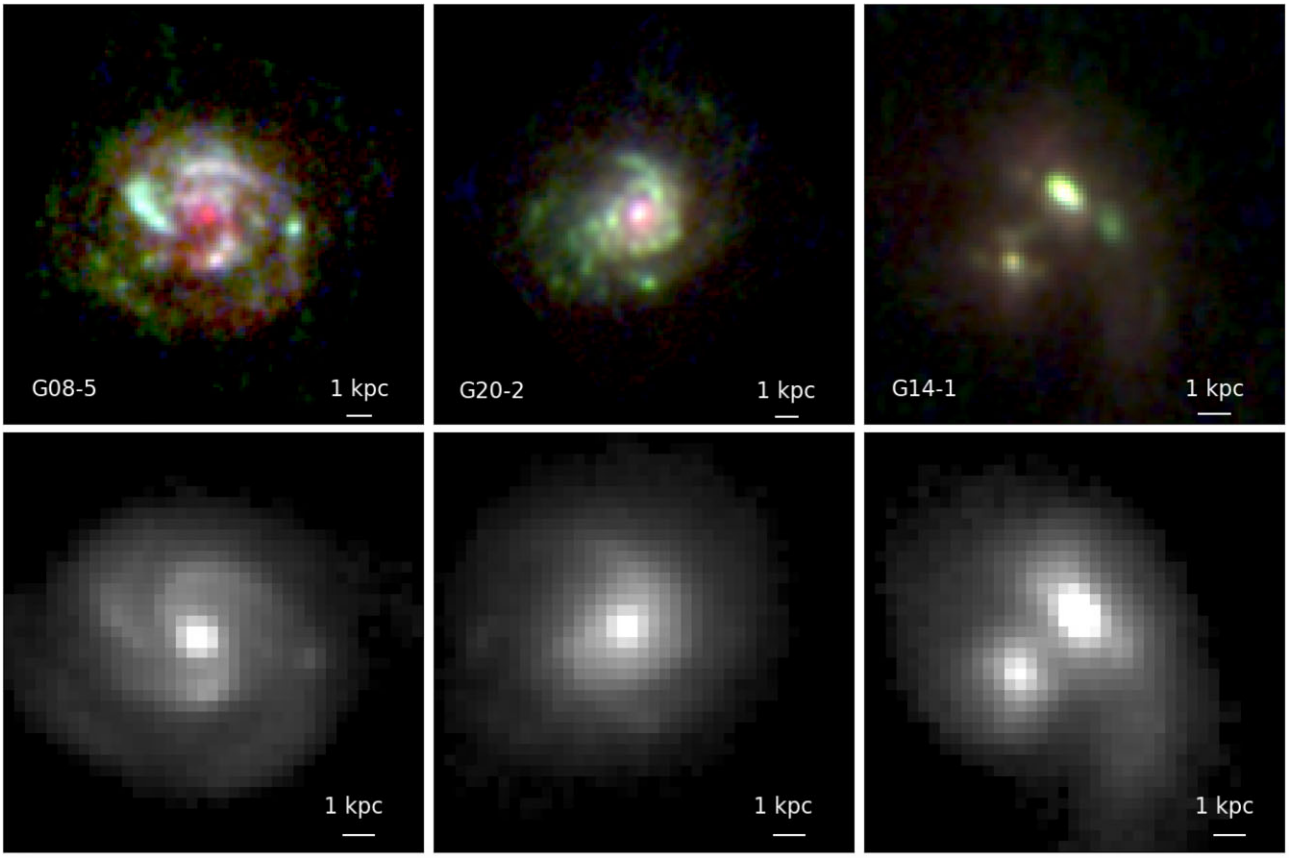


**Figure 2.** The same as Fig. 1 but for target G20-2, G14-1, and G08-5, respectively.

Moreover, based on results from Fisher et al. (2017a), it leaves clumps poorly resolved with only 1-2 WFC3/IR resolution elements per clump. We therefore test the systematic bias of using or omitting *F125W* on the derived mass-to-light ratios. If derived mass-to-light ratios without *F125W* do not differ significantly from those with *F125W* we will then opt for the higher spatial resolution measurements.

We will therefore consider two separate resolutions for our mass measurements. First, we convolve and resample all bands to match the spatial resolution of *F125W*. We then measure the mass-to-light ratio in each resolution element within the galaxy, as described in Section 3.4. Second, we convolve and resample all bands, except *F125W*, to match the spatial resolution of *FR647M*.

### 3.1 Point spread function convolution

In order to generate matched point spread function sets of images we use standard IRAF packages. We created two sets of images. The first set is matched to the UVIS/IR *F125W* resolution, which has FWHM ∼0.13 arcsec. This set of images was used to measure the mass-to-light ratio (from all bands) in each resolution element within the galaxy. We note that this is intended to investigate the direct effect of including near-IR data on mass-to-light measurement (see Fig. 8), as described above. This resolution is sufficient to identify individual clumps, but does not resolve them well (see bottom panels of Figs 1 and 2).

We, therefore, adopt the second set of images which is convolved to match the resolution of ACS/WFC *FR647M* images. This difference gives us significantly better resolution, which can be used to measure properties inside of clumps. There is a known systematic offset in the WCS positioning of the images from ACS and those from WFC3/UVIS, which we correct using standard point-source matching methods. The FWHM in the images set to match *FR647M* is 0.05 arcsec.

### 3.2 Identification of stellar clumps

Historically, clumps have been identified in either emission-line maps that trace star formation or in rest-frame blue wavelength data (*U* or *B* band). Lenkić et al. (2021) show that significant colour gradients exist inside of clumps, which implies that longer wavelength identifications of clumps will be systematically different. In this paper, we aim to identify similar young structures as in $z > 1$ systems (e.g. Jones et al. 2010; Livermore et al. 2012; Guo et al. 2015), and study the stellar mass associated with them. We, therefore, identify clumps using *F336W* (*U*-band) images. We use an unsharp masking technique similar to that developed by Fisher et al. (2017a) and not dissimilar from that used in CANDELS survey Guo et al. (2015). We opt for *F336W* as detection band rather than *NUV*-band (*F225W*) since the *F336W* image has a higher signal-to-noise ratio. Moreover, this is a similar rest-frame wavelength to that used by (Guo et al. 2015), ∼300 nm.

We refer the reader to Fig. 3 where we use target G04-1 as an example to illustrate the clump selection method. First, the *F336W* images (first panel of Fig. 3) were convolved with a Gaussian kernel with an FWHM that is eight pixels. Next, we subtract the convolved image (second panel of Fig. 3) from the original and divide the difference image by the convolved image. This image gives

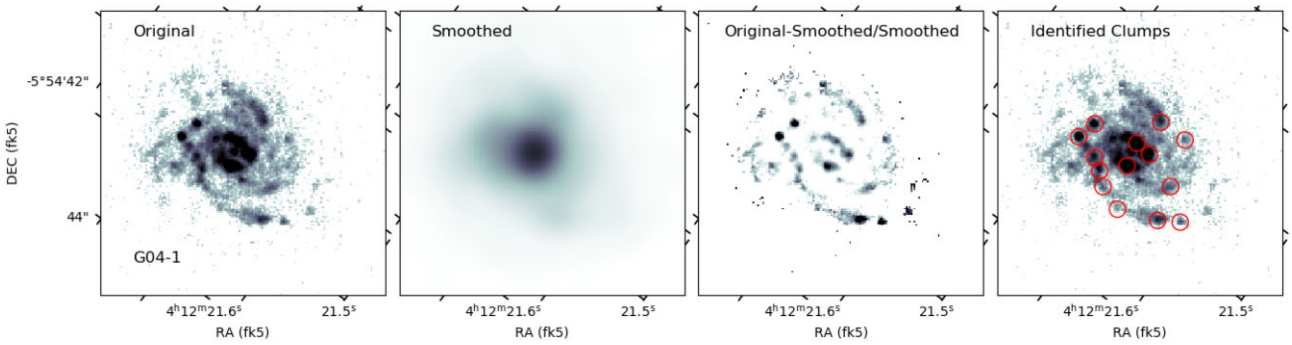


**Figure 3.** The above image illustrates various stages of clump identification in DYNAMO galaxies. Original image of galaxy G04-1 in *F336W* band, smoothed image that was created by convolving the original image by a Gaussian with eight pixels FWHM (full width at half-maximum), unsharp masked image created by subtracting the smoothed image from the original image then dividing by the smoothed image. The last panel shows all identified clumps in this galaxy.

a detection image (third panel of Fig. 3) that we use, in combination with the original image, to identify clumps.

The clumps were identified as meeting the following four criteria: (1) at least 2 times the background scatter within the region of a galaxy in the detection image; (2) at least a 5$\sigma$ peak above the galaxy disc light in the original *F336W* image; and (3) it must maintain (1) and (2) over an area of at minimum 2 × 2 pixels, a full resolution element; (4) clumps must be an independent source, that is the flux must decline in all directions from the local peak in emission.

The cut values in we use in criteria (1) are chosen to be roughly consistent with a 'by-eye' visual selection method. In the sample of six DYNAMO galaxies, we detected a total of 66 clumps. This corresponds to an average of 11 clumps per galaxy; however, the number of clumps per target ranged from 3 (G14-1) to 17 (D13-5). This is a similar number of clumps per galaxy as is observed in $z >$ 1 lensed observations (e.g. Livermore et al. 2012; Cava et al. 2017). Our aim with DYNAMO work is to recover similar properties as are observed in higher z systems, which again motivates this choice. Using a higher cut value will result in decreasing the number of clumps, and possibly biasing to higher masses. An alternate method of identifying clumps may simply be to calculate the $\Sigma_{\rm SFR}$ and size in H$\alpha$ maps, it is beyond the scope of this work to investigate this particular systematic.

Fig. 4 shows an example of the light profile of a clump in the galaxy D13-5 in three filters from different resolutions. These show that the clumps we detected are well resolved in different resolutions and bands.

### 3.3 Measurement of clump sizes and fluxes

Once clump locations are identified in *F336W* band, we then use the *F336W* to measure the size of the clumps. We used *F225W*, *F336W*, *F467M*, and *FR647M* to measure the flux of clumps. Our aim is to identify the young cluster and its extent in *F336W*, then determine its flux in all bands. We are therefore measuring the clump mass associated to young stellar population. This almost certainly introduces a systematic bias, as the size of clumps may vary as a function of stellar population. This age gradient inside of DYNAMO clumps has been studied by Lenkić et al. (2021) on the same targets. Our clump sizes should be understood as the size of the young star forming region.

In order to measure the size of clumps, we fit an elliptical Gaussian function to the 2D brightness distributions surrounding each peak in the *F336W*. The radius of each clump is then defined as the mean standard deviation of the major and minor axis of the 2D Gaussian functions (i.e. ≈FWHM/2.3553). This size is the region in which a young stellar population is exceedingly bright compared to discs. We use the same measurement technique as was previously published in Fisher et al. (2017a), see their section 3 for details.

Clump fluxes are measured in the *F225W*, *F336W*, *F467M*, and *FR647M* filters. The *FR647M* filter is a medium band ramp filter that was positioned to avoid the H$\alpha$ and [N II] emission lines. It is therefore a robust measurement of the ∼600-nm continuum flux. This provides a compromise between resolution and probing the older stellar populations.

For each identified clump, we calculate the flux by integrating the light of each pixel within a defined aperture centred on each clump. However, multiple complexities occur when measuring clump fluxes. Overlapping flux from neighbouring clumps (or the galaxy centre) and the background light from the disc are both sources of systematic uncertainty in the clump flux. We construct a method that is similar to fitting Gaussians to clumps as a means to measure the flux; however, it does not make a priori assumptions about the shape of clump surface brightness profiles. For each clump, we define a square working region that is 1.2 arcsec across, positioned at the centre of each clump. We then measure the profile of the median flux as a function of radius for each clump in each filter. If a pixel flux is significantly brighter than the median, or if it is a systematic increase in flux with radius from the clump centre, then that light is assumed to be representative of flux from the neighbouring clump. These flux values are flagged and replaced by the median value at the same radial distance from the clump centre. We find this gives very similar flux values as a Gaussian fit to each clump. We then integrate the 'processed' clump flux within the clump radius (as defined in the *F336W* images).

In order to separate the light of clumps from the diffuse components of the galaxies, we subtract a local disc flux from each clump. To measure the light from the disc that is superimposed on to the clump, we fit a Gaussian plus constant function to each clump's radial profile in each band image after the masking has taken place, and use the constant as representative of the background disc light. The disc flux is then inward extrapolated to be that value over the same area covered by the clump. We note that for physical interpretation reasons, it is not clear if the disc should be removed from clump measurements or not. If disc light is subtracted, one is implicitly assuming that clumps are distinct objects from the background light, whereas if disc light is not subtracted, clumps are simply overdense regions within a disc. The latter argument is motivated by the observation that clump sizes are of order the same thickness as the disc. We therefore carry out both, and keep track the impact of local disc subtraction on our

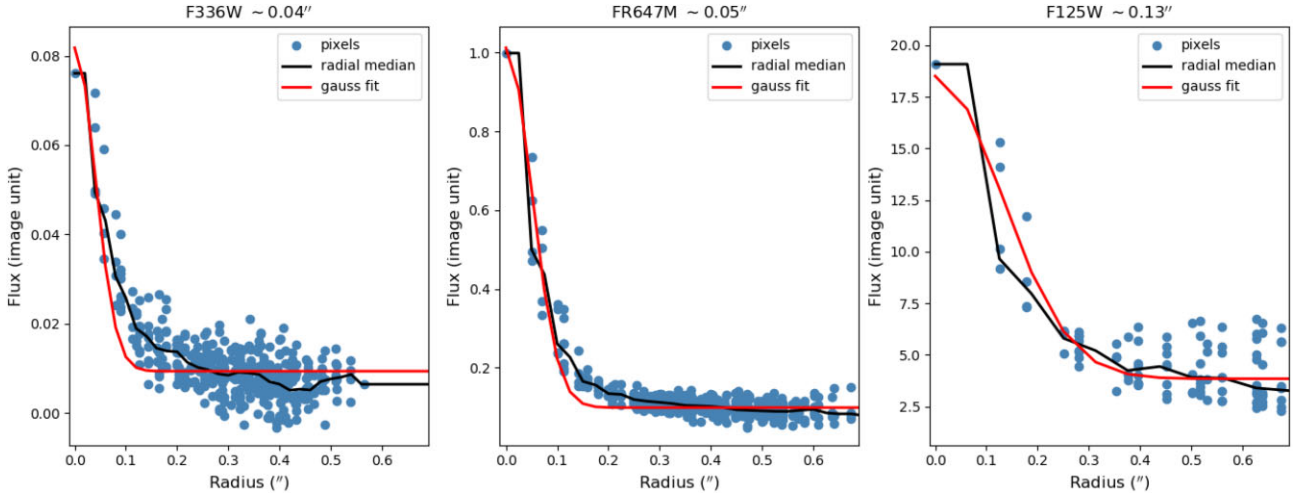


**Figure 4.** An example of light profile of a clump in *F336W* (∼0.04 arcsec), *FR647M* (∼0.05 arcsec), and *F125W* (∼0.13 arcsec) from galaxy D13-5. The red line indicates a 1D Gaussian fit to the data, and the black line represents the median radial in radial bin fit to the data. This again shows how the *F125W* data resolved clumps poorly.

main results. We record all clumps both raw, and processed and disc subtracted fluxes in each filter in Appendix A, Table A1.

In Figs 5 and 6, we assess the effect of 'processing' and disc correction on the calculated flux of clumps in each filter for all our targets. We compare the flux of the clumps after the processing and disc subtraction to the raw clumps flux (before 'processing' and disc subtraction) assuming the same size/diameter. We also compared the 'processed' clumps flux but non-disc corrected with 'processed' and disc corrected. As is clear from the figure, the effects of both local disc subtraction and the processing procedure vary only mildly with clump flux, and do not vary significantly from galaxy to galaxy. Without disc subtraction, the processed and raw clump fluxes are consistent to 10 per cent. The impact of disc subtraction is more significant, reducing the flux by a median of roughly 50–60 per cent in the *FR647M* filter. The impact is more significant for the faintest clumps, whose fluxes are reduced by a factor of ∼3-4 times, while the fluxes of the brightest clumps are reduced by a factor of 1–2 times at most.

### 3.4 Measuring stellar masses by SED fitting

We measured the stellar mass through fitting stellar population synthesis models to the observed SEDs. We used the CIGALE (Code Investigating GALaxy Emission) SED-fitting software (Boquien, M. et al. 2019) to derive physical properties of clumpy galaxies, such as stellar masses, age, and extinction. Here we note that, we performed the SED fitting on those two sets of images described in Section 3.1: (1) We ran CIGALE in each resolution element in the galaxy using all available filters from our program from WFC3/UVIS (*F225W*, *F336W*, *F467M*), ACS/WFC (*FR647M*) and WFC3/IR (*F125W*) that were matched and resampled to the resolution of the *F125W* images. We remind our reader that this is only intended to assess the effect of including near-IR (*F125W*) data on our stellar mass measurement. (2) We ran CIGALE using clump fluxes measured from WFC3/UVIS (*F225W*, *F336W*, *F467M*), and ACS/WFC (*FR647M*), that were matched and resampled to the resolution of the *FR647M* images.

For the SED fitting, we adopted the stellar tracks of Bruzual & Charlot (2003) at solar metallicity, which is close to the value measured in gas-phase metallicity with SDSS for our sample (Pettini & Pagel 2004). We adopted the Chabrier (2003) initial MF. The Calzetti et al. (2000) attenuation law is currently the most used for $z \sim 2$ galaxies. We implemented a modified Calzetti dust law and specific recipe described in Buat et al. (2012). The authors analysed a sample of strong *UV* emitting galaxies at $z \sim 2$, and found evidence for a steeper *UV* slope than is reported Calzetti et al. (2000). Following Buat et al. (2012) and Lo Faro et al. (2017), we fixed the power-law slope to −0.3 and varied E($B - V$) from 0.05 to 1.3 for young populations. We allowed the age of the main stellar population to vary between 10 and 1000 Myr, based on expectations from absorption-line studies of DYNAMO galaxies (Bassett et al. 2014).

In Fig. 7, we consider two commonly used star formation history models available in the CIGALE SED fitting code. The first is a star formation history defined by double exponentials (*sfh2exp*). In this model, a burst is superimposed on a decaying older stellar population (see Boquien, M. et al. 2019, for more in-depth discussion). In the *sfh2exp* models, we used three different assumptions for the late burst component $\tau = 10$, 100, 200 Myr. We also allowed the burst fraction to vary from 0.01 to 0.5 in each pixel. This has previously been used to measure stellar masses of high-redshift galaxies (e.g. Glazebrook et al. 2004). The second one is a delayed $\tau$ star formation history model, *sfhdelayed*, which gives a nearly linear increase of star formation until the age (the time of onset of star formation) is equal to $\tau$, then decreases exponentially (Boquien, M. et al. 2019). This star formation history model is commonly used in the literature, including in analysis of clump masses (e.g. Cava et al. 2017; Dessauges-Zavadsky et al. 2017; Guo et al. 2018). In the *sfhdelayed* model, we adopt $\tau = 10$, 30, 50, 100, 200 Myr. We note that we used the same IMF and extinction properties for both star formation history models.

The histograms in Fig. 7 show the impact that these different star formation history models have on stellar masses. We find very similar stellar mass distributions for all runs. The median stellar mass of all pixels derived from the star formation history model is $\log(M/M_\odot) = 6.9$ with standard deviation 0.46 dex. For the double exponential SFH model, we find that the median stellar mass of all pixels is $\log(M/M_\odot) = 6.9 \pm 0.47$, $7.0 \pm 0.47$, $7.1 \pm 0.46$ for $\tau = 10$, 100, 200 Myr, respectively. These results essentially reiterate the result of Taylor et al. (2011), in which they find that mass-to-light ratio is a robust quantity within SED modelling.

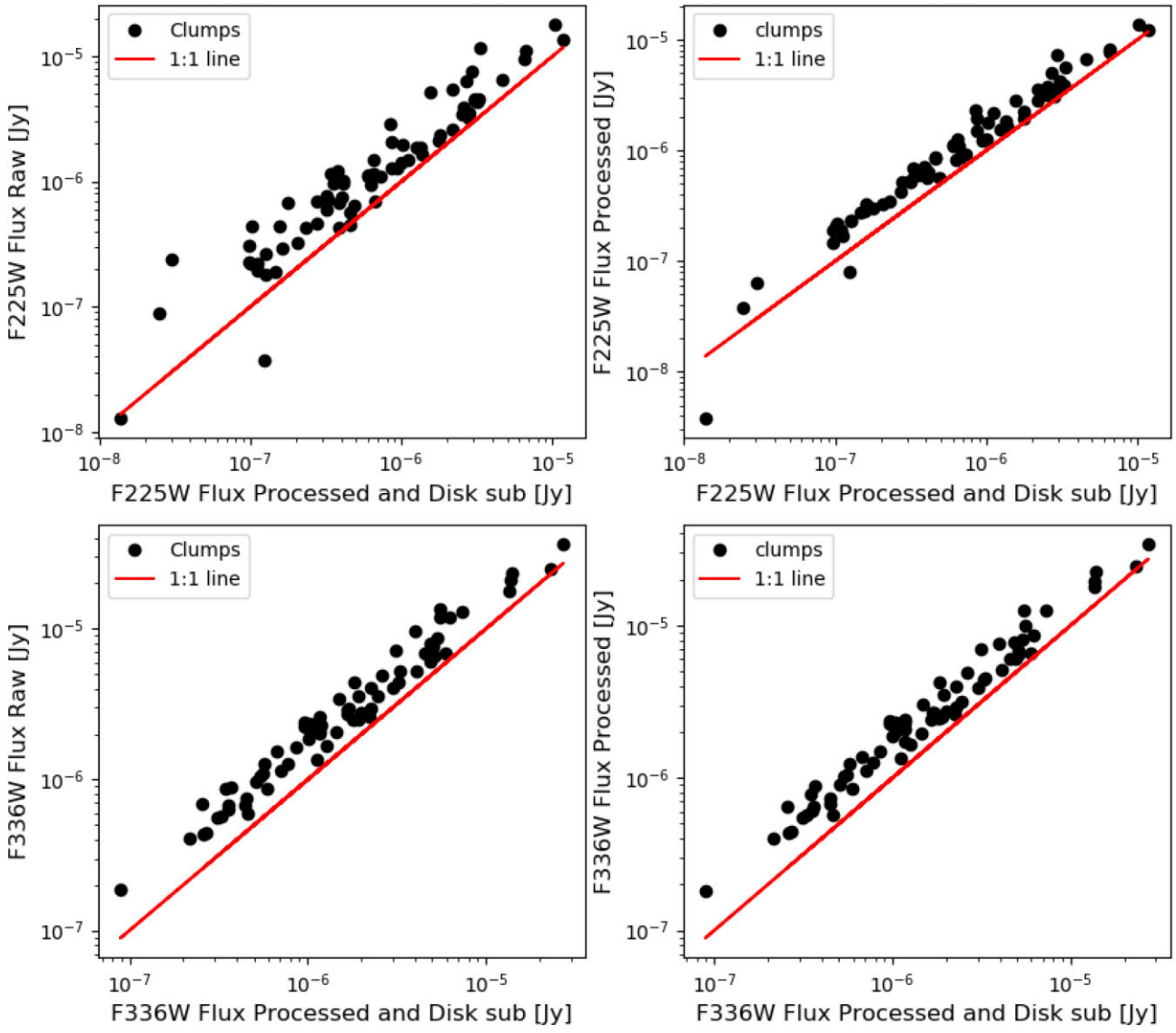


**Figure 5.** Clumps fluxes comparison in *F225W* and *F336W* filters. Left-hand panel: comparison of clumps fluxes measured before (*y*-axis) and after processing and disc subtraction (*x*-axis). Right-hand panel: comparison of clump fluxes after processing only (*y*-axis) and both processing and disc subtraction (*x*-axis). The red line indicates one-to-one relation between fluxes. The largest effect on clump flux is from disc subtraction, which reduces clump fluxes by ∼50 per cent.

We also made the same comparison for raw clumps stellar masses, and this is shown in the right-hand panel of Fig. 7. We find very similar clump stellar mass distributions for all runs. The median clump stellar mass with the SFH-delayed model is $\log(M/M_{\odot}) = 7.75$ with standard deviation 0.61 dex. For the SFH-double exponentials model, we find a median of clump stellar mass $\log(M/M_{\odot}) = 7.77 \pm 0.62$, $7.82 \pm 0.60$, $7.85 \pm 0.64$ for $\tau = 10$, 100, 200 Myr, respectively. Because we do not find a difference in mass distribution of each pixel and clumps, we opt for the simplest model, of the delayed $\tau$ models.

Furthermore, we tested our method by running CIGALE for integrated galaxy light to measure the stellar mass, age, SFR, and dust extinction of the galaxies. From our integrated measurement, we found these physical properties to be very consistent with results from previous studies of DYNAMO galaxies, using SDSS magnitudes for stellar mass, H$\alpha$ for SFR, and Balmer line series for extinction (Bassett et al. 2014, 2017; Green et al. 2014; Fisher et al. 2019).

As previously mentioned, including near-IR pass-bands significantly increases the ability to derive robust stellar population properties from SED-fitting methods (e.g. Bell & de Jong 2001; Zibetti et al. 2009). We note that measuring the near-IR light of individual clumps is unique to the DYNAMO sample, *HST* programs of $z > 1$ galaxies cannot observe rest-frame near-IR. We therefore test the accuracy of the mass-to-light ratio determination using only optical pass-bands, which can also be a comparison to biases that would be present in *HST* surveys of $z \sim 2$ galaxies. We carried out this test by simply re-running CIGALE without the WFC3/IR *F125W* filter flux and following the same procedure mentioned above. We then compared this to the mass-to-light ratio measurements using all bands (near-UV to near-IR). The mass-to-light ratio was determined simply by dividing the stellar mass by the light measured from *FR647M* band.

In Fig. 8, we compare the *FR647M* mass-to-light ratio with and without the near-IR observations. The median $\log M/L_{FR647M}$ is –0.65 with standard deviation of 0.18 when we include near-IR starlight (*F125W*-filter). We find a median of $\log M/L_{FR647M} = -0.71 \pm 0.19$ when we exclude the near-IR starlight. The difference between the

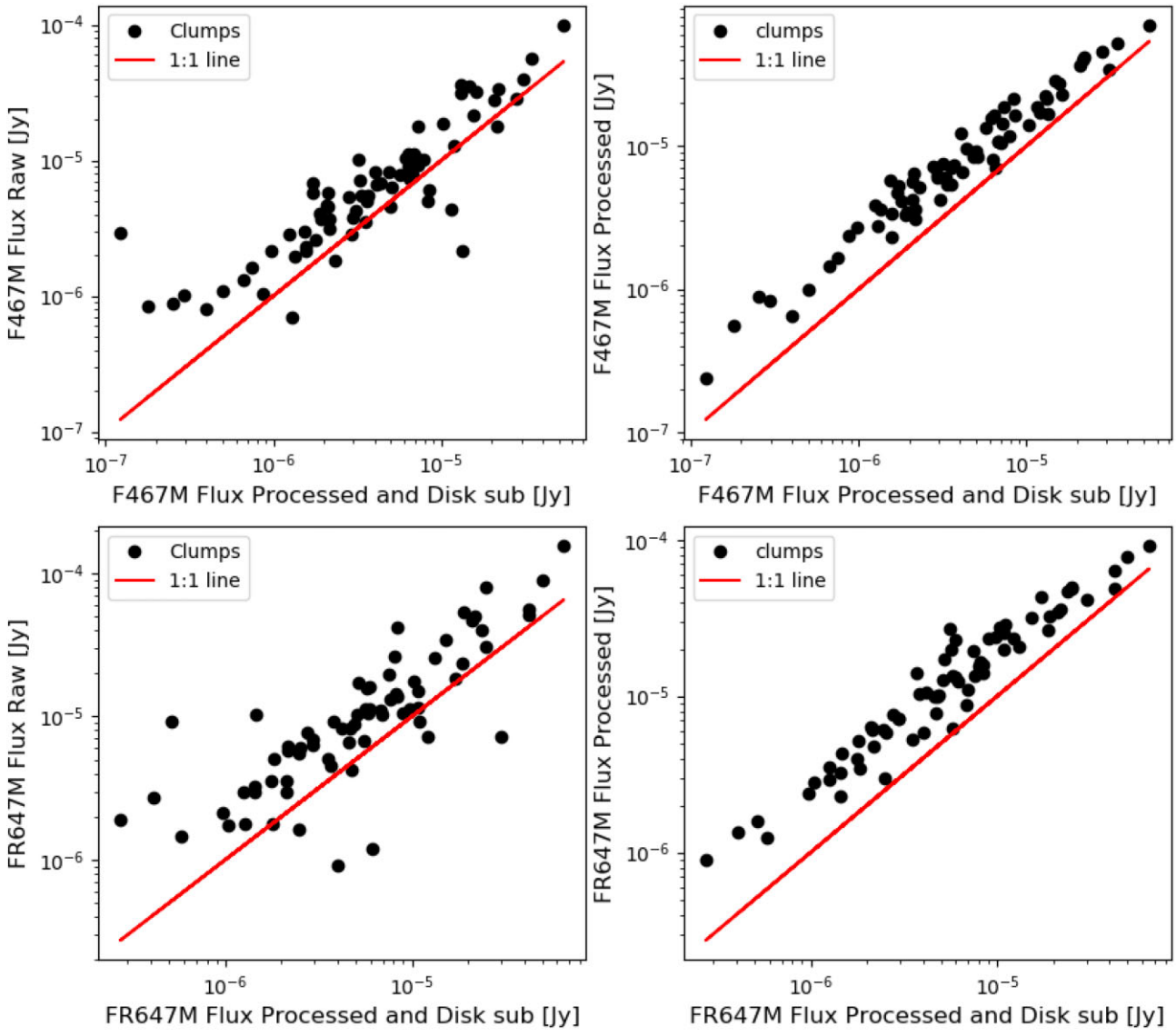


**Figure 6.** The same as Fig. 5 but for clump fluxes in the *F467M* and *FR647M* filters, respectively.

median of log M/L$_{FR647M}$ with and without *F125W* image is only 0.06 dex. This is visible in the plot, where there is only a slight tendency of log *M*/L$_{FR647M}$ to be lower when *F125W* filter is included. We note that for measuring clumps, this systematic bias is very small compared to the systematics introduced from the lower spatial resolution of *F125W*.

Because we did not find a significant difference in mass-to-light ratio when we exclude the *F125W* band, we opt to determine the stellar mass of clumps using only the finer spatial scale images [WFC3/UVIS (*F225W*, *F336W*, *F467M*) and ACS/WFC (*FR647M*], which are matched and re-sampled to the *FR647M* resolution. We also remind the reader that the resolution of *F125W* reduces our ability to resolve individual clumps by a factor of ∼2 times (see also Figs 1 and 2). Therefore, we only run CIGALE to individual clumps using their raw fluxes, and processed and disc subtracted fluxes, to determine their stellar masses. We note that we used the same well-tested CIGALE SED fit parameterization that is described in detail above.

In addition, we carried out a sanity check on how the mass-to-light ratio at a given band varies with the colour in every single pixel in the galaxy, shown in Fig. 9. In Fig. 9, we show the correlation between all pixels rest-frame colour *F336W*−*F467M* (*U* − *B*), which is an indicator of age versus mass-to-light ratio in *FR647M* band. In general, we find that blue regions have lower M/L$_{FR647M}$ whereas the redder regions have higher M/L$_{FR647M}$ as expected for this type of galaxy. This result is quite similar to Zibetti et al. (2009) found in the local Universe.

In Fig. 10, we show the distribution of mass-to-light ratios in *FR647M* band for all raw clumps (red) and for all pixels in each galaxy disc (excluding clumps; grey). We determine the mass-to-light ratio of clumps by simply taking the stellar mass of the clumps from our SED fit and dividing by the light measured from the *FR647M* band. In order to make a one-to-one comparison of clump mass-to-light ratio to the disc mass-to-light ratio, we blur the images to the average clump size. We then re-run CIGALE using the new images following the same procedure as mentioned in Section 3.4. The pixels that are co-located with the clumps in the new image were excluded from the galaxy disc. The median mass-to-light ratio of the disc population is −0.61 with a standard deviation of ±0.17.

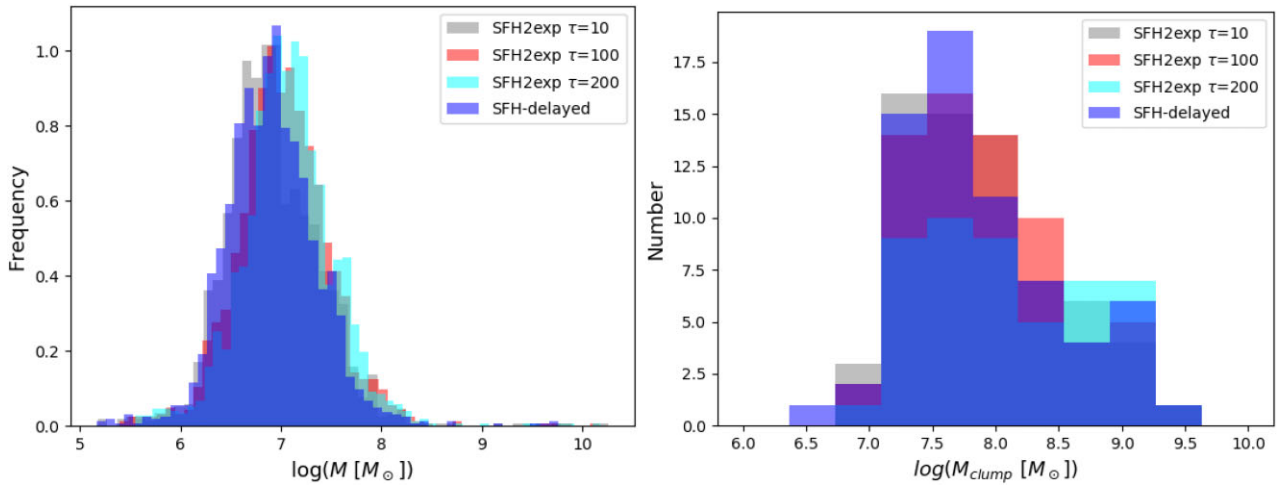


**Figure 7.** Comparison of stellar mass distribution of every single pixel (left-hand panel) and clump (right-hand panel) in all DYNAMO galaxies using two different star formation history models. The blue one is with SFH-delayed model. The grey, red, and cyan is from the double exponentials model using three different fixed $\tau$ = 10, 100, 200 Myr, respectively.

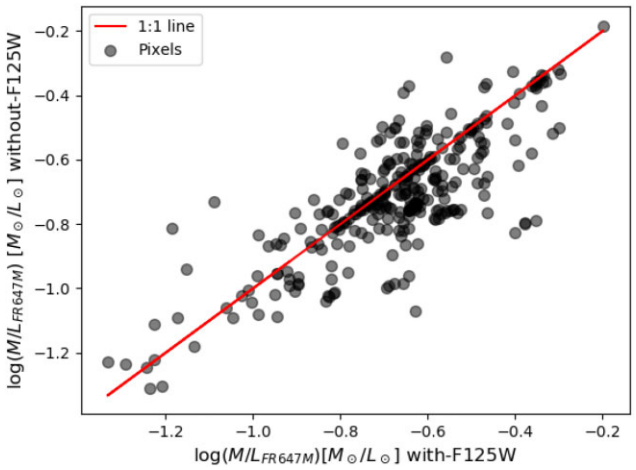


**Figure 8.** Comparison of the mass-to-light ratio in *FR647M* with and without near-IR (*F125W*) observations in every single pixel of the DYNAMO galaxy G04-1. The *x*-axis corresponds to the resulting mass-to-light ratio in the *FR647M* band when we use all five of our filters in our SED fit. The *y*-axis shows the mass-to-light ratio when we exclude the starlight from near-IR (*F125W*) observations in our SED fit. The mass-to-light ratios are nearly equal, which is shown as the red line representing the one-to-one correlation between those mass-to-light ratio measurements.

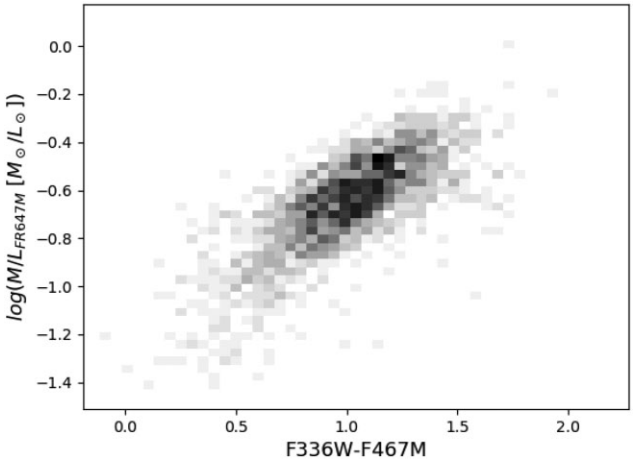


**Figure 9.** Correlation of the *F336W*−*F467M* colour and stellar mass-to-light ratio in *FR647M* band for each pixel in all DYNAMO galaxies.

Clumps are skewed towards lower mass-to-light ratios, with a median of $-0.75 \pm 0.20$. The distribution of clump $M/L_{FR647M}$ in DYNAMO galaxies is, though very broad. There appears to be a very low $M/L_{FR647M} \sim 0.1$ group of clumps and then a similar number of clumps that have comparable $M/L_{FR647M}$ to the disc light. The $M/L_{FR647M}$ peak is to some degree set by the fact that clumps are defined as peaks in blue wavelength light, and therefore younger populations. Lenkić et al. (2021) found similarly that clumps are consistent with significantly lower ages compared to the disc, and the Lenkić et al. (2021) result would suggest that the low $M/L_{FR647M}$ values are due to clumps having younger stars, rather than less extinction. In general, that clumps have low mass-to-light ratio than the discs. Clumps with $M/L_{FR647M}$ above –0.61 are 22 per cent of the entire population of clumps.

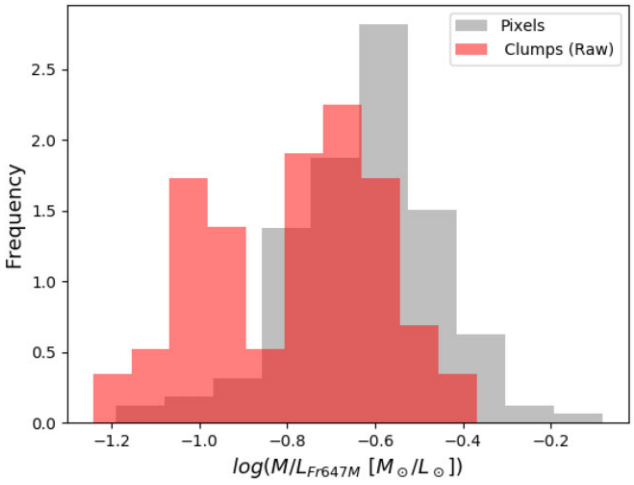


**Figure 10.** Distribution of mass-to-light ratio in *FR647M* of raw clump (red) in DYNAMO galaxies and every single pixel of DYNAMO galaxies (grey).

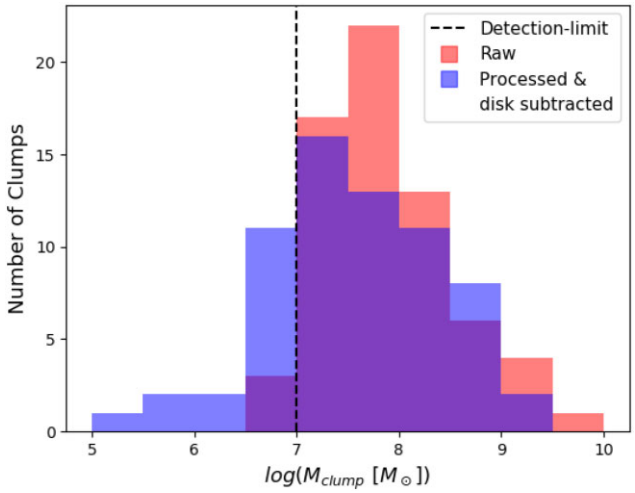


**Figure 11.** Stellar mass distribution of all clumps in our DYNAMO galaxies for raw clumps (red) and processed and disc subtracted clumps (blue). The vertical black line indicates our minimum mass detection limit in our targets, which is $\sim 10^7$ $M_\odot$. See Table A2 in Appendix A for raw clump stellar masses, and processed and disc subtracted clump stellar masses.

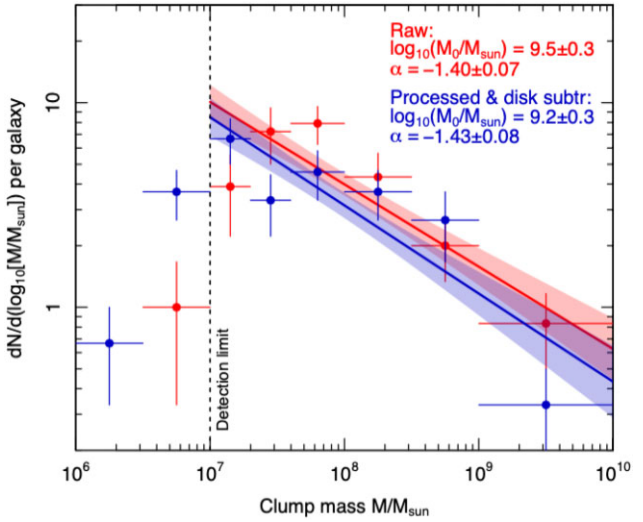


**Figure 12.** Stellar MF of all clumps in DYNAMO galaxies. The circle indicates the resulting stellar MF distribution of raw and processed and disc subtracted clumps, respectively. The solid and dash line indicate a single power-law fit to the mass. The vertical black line in both panels indicates our minimum mass detection limit in our targets, which is $\sim 10^7$ solar mass.

## 4 RESULT AND DISCUSSION

### 4.1 Stellar mass of clumps in DYNAMO galaxies

Fig. 11 shows a distribution of the stellar masses of the raw clumps, and processed and disc subtracted clumps of the DYNAMO galaxies. We find that the clump mass in our sample ranges from $4.71 \times 10^6$ to $3.74 \times 10^9$ $M_\odot$ and $2.95 \times 10^5$ to $2.03 \times 10^9$ $M_\odot$ and that the average clump mass is $2.53 \times 10^8$ and $1.60 \times 10^8$ $M_\odot$ for raw clumps, and processed and disc subtracted clumps, respectively.

The vertical solid line indicates our clump minimum mass detection limits, which is very near $\sim 10^7$ $M_\odot$. To determine the minimum mass detection limit, we take five different background regions in each galaxy assuming an aperture size of $\sim 3 \times 3$ pixels, which is the average size of a clump. We measure the mass of each background region in the galaxy, and then calculate the average equivalent 'mass' of the five background regions in each target. We then take the average equivalent mass from each target as the minimum detection mass limit. We note that the actual mass detection limit will be different for each galaxy, which has different redshifts. This limit is intended to be a rough characteristic of the detection limit for the sample. From a total of 66 clumps, only two clumps and seven clumps are below our detection limit in raw and processed and disc subtracted clumps, respectively. We note that the peak of our distribution of masses is nearest to the detection limit, which suggests that in clumpy galaxies, clumps may be the high-mass end of a continuum of masses that begins at lower masses.

Generally, we find similar mass distributions between the raw clumps, and processed and disc subtracted clumps. We obtain that on average, the processing and disc subtraction procedures reduce the clump masses by 40 per cent. We find a similar mass drop in all clumps. In addition, the impact of processing and disc correction on clump masses is similar across our targets.

Overall, we find our distribution of clump masses favours low masses, as indicated both by the peak in the histogram (Fig. 11) and the slope of the distribution in the stellar MF (Fig. 12). Theories in which clumps originate from *ex situ* source, such as mergers and accretion, suggest that clumps would favour larger masses, or at least have an increase in high masses (see discussion in Huertas-Company et al. 2020). We do not find this in the DYNAMO clump masses.

Results from simulation work show that stellar masses of clumps in turbulent, clumpy disc galaxies at $z \sim 2$ depend on the nature of the driver of stellar feedback assumed (e.g. Mandelker et al. 2016; Mayer et al. 2016). FIRE simulation results show that in high $\Sigma_{SFR}$ regions there is a strong radiation pressure, and this results in clumps that are short-lived $\leq 20$ Myr (Oklopčić et al. 2016), see also similar results with the NIHAO simulation and the impact of so-called 'early stellar feedback' (Buck et al. 2017). Mandelker et al. (2016) discuss the impact of radiation pressure prescriptions on the distribution of clump masses. In effect, only clumps that are very massive are able to survive the strong radiative feedback models. This would result in a mass distribution of clumps that is skewed to high masses, and the vast majority of clumps are disrupted by internal feedback before they are able to migrate to the galaxy centre. The DYNAMO sample tends to favour lower mass clumps. The most common mass of clumps in DYNAMO galaxies is 1–3 $\times$ $10^7$ $M_\odot$, depending whether the disc is subtracted or not.

Simulations in which stellar feedback is primarily driven by supernovae generate clumps that are long-lived with ages of 100−500 Myr and with stellar masses greater than $10^8 M_\odot$ (e.g. Bournaud et al. 2014; Mandelker et al. 2016). More specifically, Mandelker et al. (2016) finds intermediate mass clumps $10^8$–$10^{10}$ $M_\odot$ systematically increase when they include early radiative feedback compared to simulation runs without radiation pressure. The clump stellar mass in DYNAMO galaxies falls in the range of $10^6$–$10^9$ $M_\odot$, which is consistent with these simulation results. Our result is in good agreement with their 'only supernova feedback' recipe.

Observational studies at $z \sim 2$ such as Elmegreen et al. (2008), Schreiber et al. (2011), and Guo et al. (2012) obtained clumps masses of $10^8$–$10^9$ $M_\odot$. Recent work by Huertas-Company et al. (2020) on the CANDELS survey argues that observational effects such as, resolution could lead to an overestimation of clumps masses by a factor of 10, which is similar to previous estimations (Cava et al. 2017; Dessauges-Zavadsky et al. 2017; Fisher et al. 2017a).

This would be consistent with the difference in masses of a typical DYNAMO clump and those of $z \approx 1-2$ galaxies.

### 4.2 Clumps stellar MF

The rate of change in the distribution of clump masses has been studied by other authors, and is interpreted to imply clumps origin. For example, in the simplest scenario *in situ* clump origins are expected to have a more steeply declining rate of change than *ex situ* clump origins, in which some estimate an up turn in the rate of change at higher masses.

We can characterize the distribution of clump stellar masses $M$ by an MF, $\Phi(M)$. This function is defined such that the expected number of clumps per galaxy in our sample, in a small stellar mass range $[M, M + \delta M]$, is

$$\delta N = \Phi(M)\delta M. \tag{1}$$

It follows that the expected number of clumps per galaxy in the range $[x, x + \delta x]$ of logarithmic mass $x = \log_{10}(M/\mathrm{M}_{\odot})$ is

$$\delta N = \phi(x)\delta x, \tag{2}$$

with $\phi(x) = \ln(10)M\Phi(M)$. In consideration of the small galaxy sample, we limit our analysis to fitting a power-law MF,

$$\Phi(M) = \frac{1}{M_0}\left(\frac{M}{M_0}\right)^{\alpha}, \tag{3}$$

with only two free parameters, the characteristic mass scale $M_0$ and the exponent $\alpha < 0$. In logarithmic terms, this model reads

$$\phi(x) = \ln(10)\left(\frac{M}{M_0}\right)^{\alpha+1}. \tag{4}$$

Fitting such an MF to a discrete set of observed masses $M_i$ (with $i$ being the clump index) is a tricky problem, especially if the sample is relatively small. Perhaps the most intuitive method, still often used in fitting galaxy MFs, is to bin the data into regular mass or log-mass intervals and then fit the MF to the binned data using a standard fitting technique such as $\chi^2$-minimization. The downside of this approach is that it depends on the arbitrary choice of bins and often behaves badly if the bins are gradually reduced to infinitesimals. Only by carefully expressing the likelihood function using predictive Poisson statistics see (e.g. Cash 1979) in infinitesimal bins, can we make the bins disappear correctly. The exact likelihood function of the clump MF then becomes

$$\ln L = \sum_i \ln\left[N\phi(x_i)\right] - N\int \phi(x)\mathrm{d}x, \tag{5}$$

where $i$ goes over all the clumps and $N = 6$ is the total number of galaxies. This number appears in the likelihood, because we have defined the MF in such a way that it returns the distribution of clump masses *per galaxy* in the sample. For a full derivation of equation (5), please refer to equations (3)– (10) in Obreschkow et al. (2018) (note that their effective volume $V(x)$ is analogous to the number $N$ in the present case). This reference also explains how the likelihood can be generalized to account for mass measurement uncertainties. We here neglect such uncertainties, but note that identical and normally distributed measurement errors would only affect the power-law normalization $M_0$, not the index $\alpha$.

We determine the free parameters $M_0$ and $\alpha$ by maximizing equation (5), while evaluating the integral between $x = 7$ (the detection limit) and $x = 10.5$ (the approximate value of the galaxy stellar masses). The fits are obtained via the *dftools* package published by Obreschkow et al. (2018) for the *R* statistical language. This approach readily returns the maximum-likelihood solution, as well as parameter uncertainties and Bayesian evidence estimates.

The best-fitting power-law solutions with their $1\sigma$ uncertainty ranges, obtained by propagating the covariance matrix of $M_0$ and $\alpha$, are shown in Fig. 12. We show the stellar MF of the raw (red) and processed and disc subtracted clumps (blue) in DYNAMO galaxies. The black vertical line indicates our clumps minimum masses detection limit in DYNAMO galaxies. In our power-law fitting, we exclude clumps that have masses below our minimum masses detection limit to avoid incompleteness issue. We find a power-law slope of $-1.40 \pm 0.07$ and $-1.43 \pm 0.08$ for raw and processed and disc subtracted clumps.

Dessauges-Zavadsky & Adamo (2018) calculated the stellar MF of clumps in a sample of lensed galaxies at $z \sim 1-3$. They find slopes more similar to $-1.7$. This is within uncertainties from the MF power-law in local spirals, $\alpha \approx -2 \pm 0.3$ (Adamo et al. 2013). Dessauges-Zavadsky & Adamo (2018) argue that small, inhomogenous samples, similar to what we study with DYNAMO, can lead to shallower slopes than the true underlying populations of star clusters in galaxies. Dessauges-Zavadsky & Adamo (2018) used a sample of 27 galaxies with 194 clumps, which is ∼3 times larger than ours. Our sample, has the feature of being more consistent in selection of galaxy mass, and all are well studied as rotating, marginally stable discs (Fisher et al. 2017b). Recently, Huertas-Company et al. (2020) find a power law of $\alpha \approx -1.55 \pm 0.34$ for data from the VELA simulations. We do not know if the differences from DYNAMO sample is significant or due to the low number statistics of this difficult to determine quantity.

### 4.3 Mass–size relation for clumps

The size–luminosity and size–mass relationship for clumps has been studied by a number of authors (e.g. Livermore et al. (e.g. Livermore et al. 2012; Wisnioski et al. 2012; Cava et al. 2017; Fisher et al. 2017a; Cosens et al. 2018; Messa et al. 2019). In general, both H$\alpha$ flux and stellar mass have been shown to be at least roughly consistent with constant surface brightness or constant surface density. Fisher et al. (2017a) show that the zero-point of this correlation is offset and varies with galaxy SFR.

In Fig. 13, we show mass and size of all clumps in DYNAMO galaxies for both raw (red) and processed and disc subtracted (blue) clumps. The horizontal dash line indicates our minimum clump mass detection limit in DYNAMO galaxies. A power-law fit into the data results in slope ∼2.4 ± 0.22 and ∼2.3 ± 0.30 for raw and processed and disc subtracted respectively. These slopes are calculated for clumps masses above our minimum mass detection limits. We do not find a significant difference in this correlation due to effects of disc subtraction, aside from the known offset in masses. In general, our work is consistent with that of previous work (e.g. Cava et al. 2017). We note that for DYNAMO clumps we have now measured roughly the same power slope in $L_{\mathrm{H}\alpha}$–$r_{\mathrm{clump}}$ (Fisher et al. 2017a) and $M_{\mathrm{star}}$–$r_{\mathrm{clump}}$, implying this relationship is similar, between the conversion of star formation into mass. On some level, this is not surprising given the young ages of clumps. We also add the caveat that clump sizes are measured in *F336W*, which is dominated by young stars. Lenkić et al. (2021) investigate the colour gradients within clumps. They show that the sizes of clumps increase for redder wavelengths. Our aim in this paper is to characterize the stellar mass of the young star-forming clump, and this motivates the choice of *F336W*.

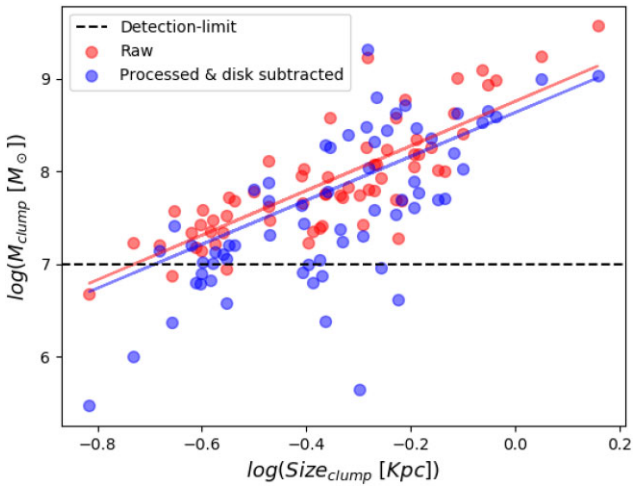


**Figure 13.** The clump stellar mass as a function of size of raw clumps (red) and processed and disc subtraction (blue) in DYNAMO galaxies. The red and blue line shows single power-law fit to the correlation for the raw and processed and disc subtraction, respectively. The horizontal dash line indicates our minimum mass detection limit in DYNAMO galaxies, which is $\sim 10^7$ solar mass.

### 4.4 Galactocentric distance gradient in clump stellar mass

In Fig. 14, we show the measured stellar masses of all DYNAMO clumps normalized by the host galaxy stellar mass as a function of clump position within the galaxy normalized to the radius that contains 85 per cent of the disc flux in the *F125W* starlight images.

The figure shows a weak trend of clump mass with galaxy position. Where towards the galaxy centre clump masses are larger ($M_{\rm clump}/M_{\rm gal} \sim 1$ per cent) and smaller clumps are more common at large radius. However, we note that the Pearson's correlation coefficient indicates a weak correlation at best ($r = -0.30$), and massive clumps ($M_{\rm clump}/M_{gal} > 1$ per cent) are observed to radii as large as ∼60 per cent of the galaxy light. Moreover, any trend in which more massive clumps are preferentially found in the galaxy centre could be a selection effect, as lower mass clumps could blend with the disc in the galaxy centre. A more informative comparison may come by comparing statistical averages to simulation results.

We compared our observations with the results from simulation by Mandelker et al. (2016) in the same figure. The simulation does not account for disc subtraction, nor anything similar to our processing algorithm. We, therefore, only consider the raw mass of clumps in this comparison. We note that this correlation remains true in the processed and disc subtracted DYNAMO clumps, taking into account those systematic differences described above. We also point out the many systematic uncertainties in comparing galaxy substructure with simulation data, as there are very significant differences in how the physical properties are determined. One source of systematic uncertainty is in the normalizing galaxy sizes. The $R_{\rm gal,85\ per\ cent}$ for DYNAMO galaxies were estimated using the *F125W* starlight, whereas, in the simulations Mandelker et al. (2016) used the 'cold mass', which will include stars and gas. We find typical $R_{\rm gal,85\ per\ cent} \sim 4-6$ kpc, which is similar to the disc sizes reported in these simulations (Mandelker et al. 2014).

In all panels, DYNAMO clumps are represented by red symbols. In the top row, we compare DYNAMO clumps to short-lived clumps from the simulation, and in the bottom row we compare to long-lived clumps. Mandelker et al. (2016) defines the boundary between long-lived and short-lived clumps as 20 times the free-fall time, which would typically correspond to ∼100−200 Myr. The left- and right-hand panels show shaded regions and coloured lines corresponding to the medians and ∼ 68 per cent of the respective samples in position (left) and mass (right).

First, we compare DYNAMO clumps to the short-lived clumps in the Mandelker et al. (2016) simulation. DYNAMO clumps are neither at a similar location within the disc, nor do they have a similar range of masses to those of short-lived clumps. We obtain a median of positions, $\log(\text{position}_{\rm clump}/R_{\rm gal,85\ per\ cent})$, for DYNAMO clumps of −0.32 with a standard deviation of 0.24. We find $0.01 \pm 0.15$ for the simulated short-lived clumps. There is almost no overlap between the majority of DYNAMO clumps and the majority of short-lived clumps, and short-lived clumps are typically located at a radius that is a factor of 2 × larger than the location of the DYNAMO clumps. Similarly, the median stellar mass of DYNAMO clumps is $\log(M_{\rm clump}/M_{\rm gal})$ is $-2.8 \pm 0.68$, which is significantly higher than the median of $-3.3 \pm 0.4$ for simulated short-lived clumps. Together the DYNAMO clumps are both more massive and located in more centrally concentrated regions that the short-lived clumps in the VELA simulation.

We now consider the populations of simulated long-lived clumps, shown in the bottom row of Fig. 14. Long-lived clumps are a much better match the position and mass of clumps in DYNAMO galaxies. We obtain a median of positions $\log(\text{position}_{\rm clump}/R_{\rm gal,85\ per\ cent})$ for simulated long-lived clumps of $-0.11 \pm 0.25$. There is overlap between the majority of DYNAMO clumps and the majority of long-lived clumps, and the difference between the median position of DYNAMO clumps is ∼0.21 dex, which is within the scatter of both. The median stellar mass $\log(M_{\rm clump}/M_{\rm gal})$ is $-2.56 \pm 0.5$ simulated long-lived clumps. The difference between the median stellar mass of DYNAMO and long-lived clumps is roughly ∼0.2 dex.

The majority of simulated short-lived clumps are faint and reside in the outskirts of the disc compared to simulated long-lived clumps. This may bias our comparison, due to the sensitivity limits of the *HST* data. Low flux clumps in the outskirts of DYNAMO discs could go undetected. We, therefore, apply a positional cut at $\log(\text{position}_{\rm clump}/R_{\rm gal,85\ per\ cent}) < 0$ for both in comparison with position and stellar mass. We note that all the above values for both the simulation and observations are determined only for the clumps that have stellar mass greater than our minimum mass detection limits (indicated in a black horizontal dash line in Fig. 14).

We obtain a median of position $\log(\text{position}_{\rm clump}/R_{\rm gal,85\ per\ cent})$ is $-0.33 \pm 0.23$ for DYNAMO and $-0.07 \pm 0.11$ for simulated short-lived clumps. We find median of stellar mass $\log(M_{\rm clump}/M_{\rm gal})$ is $-2.79 \pm 0.69$ and $-3.25 \pm 0.43$ for DYNAMO clumps and simulated short-lived clumps, respectively. The difference between the median positions DYNAMO and short-lived is ∼0.26 dex and stellar mass is ∼0.45, which is very close to median difference before we apply the positional cut. There is no significant change in the distribution of masses. There may indeed be a population of low-mass short-lived star clusters in the outer discs of DYNAMO galaxies, however, the large clumps that are detected in a way that is intended to be similar to clumps in $z > 1$ are not similar in properties to the short-lived clumps in VELA simulations.

Recently, Lenkić et al. (2021) studied the internal gradients of optical colours in DYNAMO galaxies using the same *HST* observations as we present here. They found results consistent with a complex substructure of ages, in which the centre of the clump is young and the outer part is old. They interpret these observations

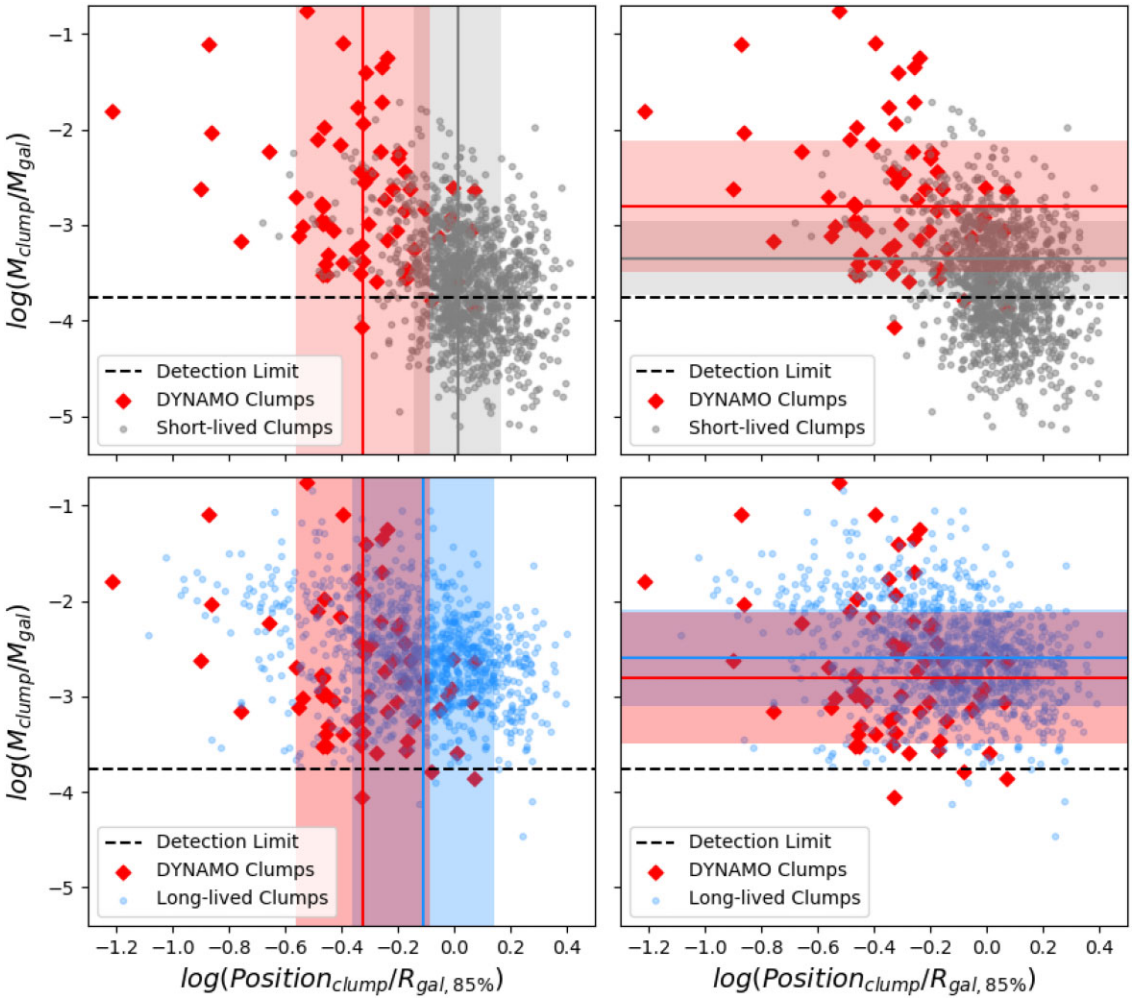


**Figure 14.** The gradient of clumps stellar masses with clumps position. The *x*-axis is clumps distance from the centre of the host galaxy normalized by a radius that contains 85 per cent starlight of the host galaxy. The *y*-axis is clumps stellar mass normalized by stellar masses of the host galaxies. In all panels DYNAMO clumps are indicated in red symbols. In the top row, we show comparison of DYNAMO clumps to short-lived (grey), and in bottom row, we compare to long-lived clumps (blue) from simulation by Mandelker et al. (2016). The coloured vertical (left-hand panel) and horizontal line (right-hand panel) indicates median of position (left-hand panel) and stellar mass (right-hand panel). The shaded area in all panels represents $\sim$ 68 per cent all respective samples position(left-hand panel) and stellar mass (right-hand panel). The shaded red and grey area encloses $\sim$ 68 per cent of DYNAMO and short-lived position of clumps, respectively. The vertical red and grey line indicates the median of DYNAMO and simulated short-lived clumps position, respectively. On the top right-hand panel, we compared the DYNAMO clumps to simulated short-lived clumps in terms of stellar mass. The shaded area encloses $\sim$ 68 per cent of DYNAMO and short-lived and long-lived stellar mass of clumps. The dash horizontal line in all panels indicates DYNAMO galaxy minimum mass detection limit.

as indicating that clumps are long-lived structures, which contain an internal centrally concentrated star formation event. This seems similar to the description of clumps in the simulations of Bournaud et al. (2014) in which clumps are long-lived and the ages based on optical star-light are continuously rejuvenated by supplies of fresh new gas. There is therefore a building of evidence that clumps in DYNAMO galaxies are more consistent with properties of long-lived clumps.

From this comparison, we conclude that the properties of DYNAMO clumps are inconsistent with the properties of simulated short-lived clumps in the VELA simulation (Mandelker et al. 2016). We find the majority of DYNAMO clumps are closer to the centre than simulated short-lived clumps and also more massive than simulated short-lived clumps. Generally, DYNAMO clumps properties are more similar to simulated long-lived than short-lived clumps, in position and stellar mass.

### 4.5 Specific SFR of clumps in DYNAMO galaxies

DYNAMO galaxies are, by selection, high specific SFR systems. They are typically more consistent with values found in $z \approx 1.5$ galaxies, rather than local spirals. White et al. (2021) show that this remains true for the resolved relationship of $\Sigma_{\rm SFR}-\Sigma_{\rm star}$ for one DYNAMO galaxy observed with Keck adaptive optics. They find $\Sigma_{\rm SFR}$ that are a factor of $\sim$2 times larger than the averages for $z \approx 1$ galaxies from the CANDELS survey (Wuyts et al. 2013). We intend to complete a full analysis of clump specific SFRs on our *HST* sample in a future work (Ambachew, in preparation), but for the purposes of discussion we will consider averages here.

We estimate the average sSFR of clumps by combining SFR measured in *Hα* observation from Fisher et al. (2017a) and stellar masses of clumps from this work. We find that in DYNAMO galaxies the average sSFR of clumps is 4.1 Gyr$^{-1}$, with an overall range of values from $\sim$0.2–7.5 Gyr$^{-1}$. This is within the range of values

observed in $z \sim 1-2$ galaxies (Wuyts et al. 2013). Mandelker et al. (2014) study the properties of clumps in $z \sim 2$ disc galaxies using adaptive mesh refinement cosmological simulation. They find the *in situ* clumps to have higher sSFR that ranges between $1-10$ Gyr$^{-1}$. Our preliminary estimation of sSFR clumps in DYNAMO galaxies is consistent with this simulation result. We will investigate this similarity in detail in our next work.

### 4.6 Implications for clump evolution

Dekel & Krumholz (2013) outline a picture in which the evolution of clumps in galaxies is largely driven by the accretion of surrounding material in the disc and the subsequent outflows due to star formation. Simulations by Bournaud et al. (2014) describe a similar picture in which clumps survive due to constant refresh of gas, in spite of the mass-loss due to strong outflows associated to high-SFR surface density regions. While DYNAMO galaxies are very similar, we have none the less determined that the mass at DYNAMO resolution is lower than early estimates of the clump masses. This may have an impact on clump evolution.

Following Dekel & Krumholz (2013), we can check the consistency of DYNAMO galaxies with this framework, in light of the results here. In order for a clump to survive in a disc, the mass accretion rate ($\dot{M}_{\rm acc}$) must be greater than the outflow mass rate ($\dot{M}_{\rm out}$) over the lifetime of the clump. We can first estimate $\dot{M}_{\rm out}$ from Dekel & Krumholz (2013) and compare to outflow rates in similar galaxies.

They state that $\dot{M}_{\rm out} \approx \eta \epsilon_{\rm ff} f_{\rm gas} M_{\rm clump}/t_{\rm ff}$. While the fiducial assumption for star formation efficiency per free-fall time is low, $\sim$0.01, Fisher et al. (2022) recently found a higher value of $\sim$0.1 in a clumpy, turbulent galaxy similar to DYNAMO galaxies, and is similar to what is observed in nearby super-star clusters. We adopt this value for the efficiency per free-fall time in our mass outflow rate estimates. We adopt $\epsilon_{\rm ff} \approx 0.1$ and similarly from Fisher et al. (2022) that $t_{ff} \approx 3-10$ Myr. Typical mass-loading factors, $\eta$, vary in clumpy galaxies. Ionized gas observations suggest $\eta \approx 0.5$ (Davies et al. 2019; Reichardt Chu et al. 2022), adjusting for molecular gas we adopt $\eta \approx 1$. We can then take the typical DYNAMO gas fraction as $f_{\rm gas} \approx 0.2$ and the average clump mass from this paper of $3 \times 10^8$ M$_\odot$. Taken together this gives a mass outflow rate for clumps of $\dot{M}_{\rm out} \approx 0.5-1$ M$_\odot$ yr$^{-1}$. This is similar to observations of mass-outflow rates in clumpy, star forming disc galaxies (e.g. Reichardt Chu et al. 2022).

The mass accretion rate of clumps in DYNAMO galaxies is challenging to measure. We will follow Dekel & Krumholz (2013) and determine if this is below the estimated outflow rate. They derive $\dot{M}_{\rm out} \approx \alpha/2(t_{\rm ff}/t_{\rm d}) M_{\rm clump}/t_{\rm ff}$. In this case, both $\alpha$ and $t_{ff}/t_d$ are taken as constants of $\sim$1/3. For the same assumption on clump mass and $t_{\rm ff}$, we derive a comparable $\dot{M}_{\rm acc} \approx 1-2$ M$_\odot$ yr$^{-1}$. This is very similar to the outflow rates but higher and, if true, implies that many clumps would be consistently long-lived as they slowly accrete more mass than they expel over their lifetime.

Multiphase outflow measurements of clumps in galaxies like DYNAMO (and $z \approx 1.5$ discs) are a direly needed observation. More work in this area, perhaps with JWST and ALMA would be critical to study the evolution of clumps in this important phase of galaxy evolution.

## 5 SUMMARY

We have studied the stellar masses of clumps in gas-rich, turbulent disc galaxies from the DYNAMO sample, which are similar in properties to $z \sim 1.5$ galaxies. DYNAMO galaxy observations allow us to study clumps with reduced uncertainty due to finer spatial resolution and measuring the star light at longer wavelengths where the mass-to-light ratio is more robust against extinction and age effects. We used a sample of six DYNAMO galaxies observed with *HST* and identified 66 clumps in *F336W* (young stars).

We find the stellar mass of DYNAMO clumps ranges from $0.04-37.4 \times 10^8$M$_\odot$ (alternatively $0.002-20.3 \times 10^8$M$_\odot$ for disc subtracted clumps). This is consistent with the finding of clumps stellar mass in observation of lensed galaxies (Cava et al. 2017). This is also consistent with VELA simulation mass threshold when they use only supernova as a feedback recipe (Mandelker et al. 2016). We measured the power-law slope of the stellar MF of the entire sample of clumps to be $\alpha - 1.40 \pm 0.07$, with little dependence on disc subtraction. This declining power-law slope is consistent with simulation work by Huertas-Company et al. (2020). We also observed a clear trend with clumps stellar mass increasing with the size of the clump. This is consistent with the findings of (Cava et al. 2017) in gravitational lensed galaxies.

We compare our observations with results from the VELA simulation (Mandelker et al. 2016). Specifically, we compare clump stellar mass to the position in the galaxy. Mandelker et al. (2016) revealed that the lifetime of the clump is connected to its position, where clumps in the central $\sim$50 per cent of the galaxy are almost always 'long-lived' clumps, and short-lived clumps are restricted to a large radius. Moreover, the stellar masses of long-lived clumps are systematically higher than those of short-lived clumps by a factor of a few. We find the masses and galactocentric positions of DYNAMO clumps are inconsistent with simulated short-lived clumps. However, clumps in DYNAMO galaxies are more similar to simulated long-lived clumps than simulated short-lived clumps.

Observations of clumps in rest-frame near-IR light will soon be possible with JWST, at least at $z \sim 1$. Our results, therefore can be tested in upcoming GTO and ERS programs. We note, however, that even with JWST the FWHM of rest-frame *J*-band light is of order 0.6–0.8 kpc at $z \sim 1.5$, which is larger than the typical size of clumps in either DYNAMO galaxies or lensed galaxies. It will, therefore, still remain challenging to isolate individual clumps. More work is still needed to determine how the biases in resolution may impact upcoming results from JWST.

## ACKNOWLEDGEMENTS

We are grateful to Nir Mandelkar for making simulation results available to us. DBF is thankful to Sarah Busch for technical help. DBF acknowledges support from Australian Research Council (ARC) Future Fellowship FT170100376 and ARC Discovery Program grant DP130101460. ADB acknowledges partial support form NSF-AST2108140. Parts of this research were supported by the Australian Research Council Centre of Excellence for All Sky Astrophysics in 3 Dimensions (ASTRO 3D), through project number CE170100013. KG is a recipient of an Australian Research Council Laureate Fellowship (FL180100060) funded by the Australian Government DO is a recipient of an Australian Research Council Future Fellowship (FT190100083) funded by the Australian Government. ID acknowledges the support of the Canada Research Chair Program and the Natural Sciences and Engineering Research Council of Canada (NSERC, funding reference number RGPIN-2018–05425).

## DATA AVAILABILITY

The DYNAMO *HST* data used in this paper are part of the Cycle 25 program 15069 and Cycle 20 program 12977, and are publicity available on the *HST* archive (https://archive.stsci.edu/hst/search.php).

## REFERENCES


Abraham R. G., Tanvir N. R., Santiago B. X., Ellis R. S., Glazebrook K., Bergh S. v. d., 1996, MNRAS, 279, L47
Adamo A., Östlin G., Bastian N., Zackrisson E., Livermore R. C., Guaita L., 2013, AJ, 766, 105
Adelman-McCarthy J. K. et al., 2006, ApJS, 162, 38
Bassett R. et al., 2014, MNRAS, 442, 3206
Bassett R. et al., 2017, MNRAS, 467, 239
Behrendt M., Burkert A., Schartmann M., 2016, ApJ, 819, L2
Bell E. F., de Jong R. S., 2001, ApJ, 550, 212
Boquien M., Burgarella D. Roehlly Y., Buat V. Ciesla L., Corre D. Inoue A. K., Salas H., 2019, A&A, 622, A103
Bournaud F. et al., 2014, ApJ, 780, 57
Bournaud F., Elmegreen B. G., Elmegreen D. M., 2007, ApJ, 670, 237
Bruzual G., Charlot S., 2003, MNRAS, 344, 1000
Buat V. et al., 2012, A&A, 545, A141
Buck T., Macciò A. V., Obreja A., Dutton A. A., Domínguez-Tenreiro R., Granato G. L., 2017, MNRAS, 468, 3628
Calzetti D., Armus L., Bohlin R. C., Kinney A. L., Koornneef J., Storchi-Bergmann T., 2000, ApJ, 533, 682
Cash W., 1979, ApJ, 228, 939
Catinella B., Cortese L., 2015, MNRAS, 446, 3526
Cava A. et al., 2017, Nat. Astron., 2, 76
Ceverino D., Dekel A., Bournaud F., 2010, MNRAS, 404, 2151
Chabrier G., 2003, Publ. Astron. Soc. Pac., 115, 763
Conselice C. J., Bershady M. A., Dickinson M., Papovich C., 2003, AJ, 126, 1183
Cortese L., Catinella B., Janowiecki S., 2017, ApJ, 848, L7
Cosens M. et al., 2018, ApJ, 869, 11
Cowie L. H. E.. S., 1995, AJ, 110, 1576
Daddi E. et al., 2015, A&A, 577, A46
Davies R. L. et al., 2019, ApJ, 873, 122
Dekel A., Krumholz M. R., 2013, MNRAS, 432, 455
Dekel A., Sari R., Ceverino D., 2009, ApJ, 703, 785
Dessauges-Zavadsky M., Adamo A., 2018, MNRAS, 479, L118
Dessauges-Zavadsky M., Schaerer D., Cava A., Mayer L., Tamburello V., 2017, ApJ, 836, L22
Elmegreen B. G., Elmegreen D. M., 2005, ApJ, 627, 632
Elmegreen B. G., Bournaud F., Elmegreen D. M., 2008, ApJ, 688, 67
Espejo Salcedo J. M., Glazebrook K., Fisher D. B., Sweet S. M., Obreschkow D., Swinbank A. M., Gillman S., Tiley A. L., 2022, MNRAS, 509, 2318
Fisher D. B. et al., 2014, ApJ, 790, L30
Fisher D. B. et al., 2017a, ApJ, 839, L5
Fisher D. B. et al., 2017b, ApJ, 839, L5
Fisher D. B., Bolatto A. D., White H., Glazebrook K., Abraham R. G., Obreschkow D., 2019, ApJ, 870, 46
Fisher D. B., Bolatto A. D., Glazebrook K., Obreschkow D., Obreschkow R. G., Kacprzak G. G., Nielsen N. M., 2022, ApJ, preprint (arXiv:2202.00024)
Genzel et al., 2006, Nature, 442, 786
Genzel R. et al., 2011, ApJ, 733, 101
Girard M. et al., 2021, ApJ, 909, 12
Glazebrook K. et al., 2004, Nature, 430, 181
Green A. W. et al., 2014, MNRAS, 437, 1070
Guo Y. et al., 2015, ApJ, 800, 39
Guo Y. et al., 2018, ApJ, 853, 108
Guo Y., Giavalisco M., Ferguson H. C., Cassata P., Koekemoer A. M., 2012, ApJ, 757, 120
Hopkins A. M., Beacom J. F., 2006, ApJ, 651, 142
Hopkins P. F., Kereš D., Murray N., Quataert E., Hernquist L., 2012, MNRAS, 427, 968
Huertas-Company M. et al., 2020, MNRAS, 499, 814
Inoue S., Yoshida N., 2018, MNRAS, 474, 3466
Jones T. A., Swinbank A. M., Ellis R. S., Richard J., Stark D. P., 2010, MNRAS, 404, 1247
Lenkić L., Bolatto A. D., Fisher D. B., Glazebrook K., Obreschkow D., Abraham R., Ambachew L., 2021, MNRAS, 506, 3916
Livermore R. C. et al., 2012, MNRAS, 427, 688
Livermore et al., 2015, MNRAS, 450, 1812
Lo Faro B., Buat V., Roehlly Y., Alvarez-Marquez J., Burgarella D., Silva L., Efstathiou A., 2017, MNRAS, 472, 1372
Madau P., Dickinson M., 2014, Ann. Rev. Astron. Astrophys., 52, 415
Mandelker N., Dekel A., Ceverino D., Tweed D., Moody C. E., Primack J., 2014, MNRAS, 443, 3675
Mandelker N., Dekel A., Ceverino D., DeGraf C., Guo Y., Primack J., 2016, MNRAS, 464, 635
Mayer L., Tamburello V., Lupi A., Keller B., Wadsley J., Madau P., 2016, ApJ, 830, L13
Messa M., Adamo A., Östlin G., Melinder J., Hayes M., Bridge J. S., Cannon J., 2019, MNRAS, 487, 4238
Noguchi M., 1999, ApJ, 514, 77
Obreschkow D. et al., 2015, ApJ, 815, 97
Obreschkow D., Murray S. G., Robotham A. S. G., Westmeier T., 2018, MNRAS, 474, 5500
Oklopčić A., Hopkins P. F., Feldmann R., Kereš D., Faucher-Giguère C.-A., Murray N., 2016, MNRAS, 465, 952
Oliva-Altamirano P., Fisher D. B., Glazebrook K., Wisnioski E., Bekiaris G., Bassett R., Obreschkow D., Abraham R., 2017, MNRAS, 474, 522
Pettini M., Pagel B. E. J., 2004, MNRAS, 348, L59
Reichardt Chu B. et al., 2022, MNRAS, 511, 5782
Saintonge A. et al., 2012, ApJ, 758, 73
Schreiber N. M. F. et al., 2009, ApJ, 706, 1364
Schreiber N. M. F. et al., 2011, ApJ, 739, 45
Shapiro K. L. et al., 2008, ApJ, 682, 231
Swinbank A. M. et al., 2017, MNRAS, 467, 3140
Tacconi L. J. et al., 2013, ApJ, 768, 74
Tacconi L. J. et al., 2018, ApJ, 853, 179
Tamburello V., Rahmati A., Mayer L., Cava A., Dessauges-Zavadsky M., Schaerer D., 2017, MNRAS, 468, 4792
Taylor E. N. et al., 2011, MNRAS, 418, 1587
White H. A. et al., 2017, ApJ, 846, 35
White H. A., Fisher D. B., Abraham R. G., Glazebrook K., Obreschkow D., 2021, AJ, 926, 14
Wisnioski E., Glazebrook K., Blake C., Poole G. B., Green A. W., Wyder T., Martin C., 2012, MNRAS, 422, 3339
Wuyts S. et al., 2013, ApJ, 779, 135
Zibetti S., Charlot S., Rix H.-W., 2009, MNRAS, 400, 1181


## APPENDIX: CLUMP PROPERTIES

**Table A1.** Fluxes of clumps in DYNAMO galaxies both raw and processed and disc subtracted in all filters.

| ID | RA | Dec. | $F_{F225W}$ (Raw) | $F_{F225W}$ (Disc sub) | $F_{F336W}$ (Raw) | $F_{F336W}$ (Disc sub) | $F_{F467M}$ (Raw) | $F_{F467M}$ (Disc sub) | $F_{FR647M}$ (Raw) | $F_{FR647M}$ (Disc sub) |
|---|---|---|---|---|---|---|---|---|---|---|
| D13-5 | | | ($\mu Jy$) | ($\mu Jy$) | ($\mu Jy$) | ($\mu Jy$( | ($\mu Jy$) | ($\mu Jy$) | ($\mu Jy$) | ($\mu Jy$) |
| 1 | 13:30:07.120 | +00:31:54.07 | 3.56 | 2.82 | 6.85 | 5.92 | 8.97 | 6.32 | 11.12 | 6.84 |
| 2 | 13:30:07.173 | +00:31:53.59 | 1.01 | 0.41 | 2.09 | 1.04 | 4.64 | 2.07 | 7.23 | 30.29 |
| 3 | 13:30:07.079 | +00:31:52.35 | 1.86 | 1.35 | 4.40 | 3.24 | 8.18 | 4.86 | 11.35 | 5.98 |
| 4 | 13:30:07.061 | +00:31:52.11 | 3.43 | 2.51 | 5.20 | 3.29 | 7.80 | 6.73 | 8.28 | 4.69 |
| 5 | 13:30:07.046 | +00:31:52.12 | 11.16 | 6.61 | 20.90 | 13.68 | 34.02 | 21.88 | 41.72 | 8.37 |
| 6 | 13:30:07.051 | +00:31:52.22 | 9.57 | 6.53 | 17.87 | 13.51 | 28.04 | 20.77 | 34.22 | 15.23 |
| 7 | 13:30:07.013 | +00:31:54.29 | 1.11 | 0.73 | 2.79 | 1.99 | 5.51 | 3.68 | 9.15 | 3.81 |
| 8 | 13:30:06.988 | +00:31:54.32 | 1.22 | 0.38 | 4.04 | 2.28 | 10.06 | 3.20 | 19.52 | 7.48 |
| 9 | 13:30:06.956 | +00:31:53.97 | 1.15 | 0.34 | 3.43 | 1.49 | 9.32 | 7.32 | 17.03 | 5.18 |
| 10 | 13:30:06.990 | +00:31:51.91 | 1.50 | 0.65 | 3.59 | 1.92 | 7.80 | 5.69 | 10.23 | 1.47 |
| 11 | 13:30:06.979 | +00:31:52.31 | 1.96 | 1.02 | 4.96 | 2.60 | 11.26 | 6.43 | 18.44 | 17.10 |
| 12 | 13:30:06.927 | +00:31:52.84 | 0.22 | 0.10 | 0.70 | 0.25 | 1.97 | 1.34 | 2.70 | 0.41 |
| 13 | 13:30:06.905 | +00:31:53.38 | 0.44 | 0.10 | 1.87 | 1.01 | 5.33 | 2.79 | 10.45 | 8.97 |
| 14 | 13:30:06.938 | +00:31:50.59 | 0.19 | 0.15 | 0.87 | 0.59 | 3.13 | 2.15 | 5.57 | 2.50 |
| 15 | 13:30:06.878 | +00:31:50.96 | 0.47 | 0.27 | 1.16 | 0.71 | 2.18 | 0.97 | 3.26 | 1.44 |
| 16 | 13:30:07.199 | +00:31:54.79 | 1.47 | 1.11 | 2.42 | 0.97 | 6.87 | 1.72 | 9.24 | 0.52 |
| 17 | 13:30:07.185 | +00:31:56.12 | 0.20 | 0.11 | 0.45 | 0.27 | 1.10 | 0.50 | 1.47 | 0.58 |
| D15-3 | | | | | | | | | | |
| 1 | 15:34:35.295 | –00:28:45.24 | 1.86 | 1.25 | 4.06 | 3.01 | 6.63 | 4.10 | 10.65 | 5.81 |
| 2 | 15:34:35.308 | –00:28:45.22 | 0.97 | 0.41 | 2.74 | 1.66 | 4.60 | 2.11 | 7.73 | 2.75 |
| 3 | 15:34:35.329 | –00:28:45.74 | 0.23 | 0.10 | 0.57 | 0.33 | 0.88 | 0.25 | 1.89 | 0.27 |
| 4 | 15:34:35.406 | –00:28:46.04 | 0.64 | 0.49 | 1.68 | 1.27 | 3.74 | 1.94 | 6.01 | 2.52 |
| 5 | 15:34:35.422 | –00:28:45.23 | 0.01 | 0.01 | 0.59 | 0.46 | 7.34 | 6.52 | 15.78 | 5.73 |
| 6 | 15:34:35.454 | –00:28:45.14 | 0.18 | 0.13 | 0.68 | 0.36 | 1.81 | 2.32 | 3.58 | 2.13 |
| 7 | 15:34:35.351 | –00:28:44.40 | 0.27 | 0.13 | 1.04 | 0.54 | 2.98 | 1.54 | 6.75 | 5.55 |
| 8 | 15:34:35.384 | –00:28:43.83 | 0.70 | 0.28 | 2.34 | 1.04 | 8.28 | 4.04 | 16.27 | 5.96 |
| 9 | 15:34:35.344 | –00:28:43.19 | 0.31 | 0.10 | 1.11 | 0.56 | 2.89 | 1.24 | 6.15 | 2.15 |
| 10 | 15:34:35.440 | –00:28:43.54 | 0.96 | 0.36 | 2.88 | 1.67 | 6.04 | 8.46 | 11.20 | 9.74 |
| 11 | 15:34:35.453 | –00:28:43.46 | 0.68 | 0.39 | 2.03 | 1.18 | 3.80 | 2.96 | 6.92 | 2.96 |
| 12 | 15:34:35.374 | –00:28:42.74 | 0.95 | 0.63 | 2.96 | 2.27 | 5.51 | 3.36 | 8.75 | 4.90 |
| G04-1 | | | | | | | | | | |
| 1 | 04:12:19.749 | –05:54:47.13 | 1.42 | 1.00 | 2.50 | 1.84 | 3.66 | 2.15 | 5.10 | 1.84 |
| 2 | 04:12:19.758 | –05:54:47.73 | 2.09 | 0.86 | 4.39 | 1.83 | 10.33 | 6.18 | 17.55 | 10.33 |
| 3 | 04:12:19.773 | –05:54:48.04 | 1.13 | 0.61 | 2.31 | 1.18 | 5.06 | 8.30 | 9.21 | 11.04 |
| 4 | 04:12:19.789 | –05:54:48.37 | 0.68 | 0.18 | 1.54 | 0.68 | 4.37 | 11.51 | 7.26 | 12.25 |
| 5 | 04:12:19.805 | –05:54:48.99 | 0.71 | 0.32 | 1.27 | 0.57 | 3.51 | 3.53 | 6.38 | 2.94 |
| 6 | 04:12:19.781 | –05:54:49.92 | 1.67 | 1.37 | 2.52 | 1.92 | 4.57 | 4.97 | 6.55 | 4.59 |
| 7 | 04:12:19.760 | –05:54:50.42 | 0.43 | 0.23 | 0.67 | 0.45 | 1.32 | 0.67 | 1.76 | 1.27 |
| 8 | 04:12:19.740 | –05:54:48.56 | 3.89 | 2.55 | 8.06 | 4.85 | 17.73 | 21.53 | 30.53 | 25.08 |
| 9 | 04:12:19.704 | –05:54:48.81 | 4.38 | 3.07 | 8.74 | 5.32 | 21.67 | 15.65 | 40.43 | 23.87 |
| 10 | 04:12:19.698 | –05:54:48.34 | 5.46 | 2.18 | 12.86 | 7.31 | 35.11 | 14.73 | 80.70 | 24.93 |
| 11 | 04:12:19.647 | –05:54:48.56 | 1.29 | 0.86 | 2.62 | 1.18 | 6.87 | 4.37 | 11.63 | 10.81 |
| 12 | 04:12:19.722 | –05:54:49.70 | 1.10 | 0.60 | 2.27 | 0.96 | 5.79 | 1.70 | 10.21 | 5.13 |
| 13 | 04:12:19.648 | –05:54:49.27 | 0.24 | 0.03 | 0.88 | 0.37 | 2.17 | 13.44 | 4.52 | 3.70 |
| 14 | 4:12:19.7189 | –05:54:47.289 | 1.29 | 0.94 | 2.51 | 1.80 | 4.07 | 1.91 | 5.82 | 2.17 |
| G20-2 | | | | | | | | | | |
| 1 | 20:44:02.988 | -06:46:56.35 | 0.75 | 0.40 | 1.28 | 0.78 | 1.64 | 0.75 | 2.97 | 1.25 |
| 2 | 20:44:03.013 | -06:46:57.61 | 1.16 | 0.65 | 1.65 | 0.86 | 2.59 | 1.79 | 3.54 | 1.77 |
| 3 | 20:44:02.965 | -06:46:57.34 | 5.13 | 1.55 | 9.71 | 3.99 | 17.73 | 7.22 | 26.06 | 8.04 |
| 4 | 20:44:03.020 | -06:46:58.08 | 0.57 | 0.46 | 0.98 | 0.51 | 2.82 | 2.92 | 2.97 | 2.12 |
| 5 | 20:44:02.950 | -06:46:57.49 | 11.63 | 3.31 | 23.42 | 13.94 | 56.73 | 34.76 | 89.36 | 49.92 |
| 6 | 20:44:02.959 | -06:46:58.07 | 6.28 | 2.67 | 11.96 | 5.55 | 31.53 | 13.20 | 50.04 | 21.77 |
| 7 | 20:44:02.984 | -06:46:58.60 | 2.14 | 1.77 | 2.60 | 2.22 | 4.24 | 3.07 | 5.02 | 3.54 |
| 8 | 20:44:02.925 | -06:46:57.83 | 2.90 | 0.84 | 7.12 | 3.14 | 28.45 | 27.90 | 50.83 | 42.64 |
| 9 | 20:44:02.944 | -06:46:58.30 | 7.60 | 2.91 | 13.51 | 5.50 | 35.84 | 12.99 | 53.89 | 19.14 |
| 10 | 20:44:02.923 | -06:46:58.44 | 4.50 | 3.07 | 7.64 | 5.07 | 18.70 | 10.28 | 25.78 | 13.19 |
| 11 | 20:44:02.906 | -06:46:58.25 | 6.49 | 4.61 | 12.02 | 6.22 | 32.02 | 16.14 | 47.34 | 21.14 |
| 12 | 20:44:02.895 | -06:46:57.80 | 18.02 | 10.27 | 36.41 | 27.26 | 99.79 | 53.69 | 155.33 | 65.25 |
| G08-5 | | | | | | | | | | |
| 1 | 8:54:18.829 | + 6:46:20.679 | 0.33 | 0.20 | 0.63 | 0.36 | 1.04 | 0.87 | 2.12 | 0.97 |
| 2 | 8:54:18.820 | + 6:46:20.533 | 0.45 | 0.46 | 0.88 | 0.35 | 2.15 | 1.57 | 4.21 | 4.77 |
| 3 | 8:54:18.788 | + 6:46:19.895 | 0.44 | 0.16 | 2.05 | 1.44 | 5.05 | 3.59 | 10.26 | 6.91 |

**Table A1** *– continued*

| ID<br>D13-5 | RA | Dec. | $F_{F225W}$ (Raw) ($\mu Jy$) | $F_{F225W}$ (Disc sub) ($\mu Jy$) | $F_{F336W}$ (Raw) ($\mu Jy$) | $F_{F336W}$ (Disc sub) ($\mu Jy$( | $F_{F467M}$ (Raw) ($\mu Jy$) | $F_{F467M}$ (Disc sub) ($\mu Jy$) | $F_{FR647M}$ (Raw) ($\mu Jy$) | $F_{FR647M}$ (Disc sub) ($\mu Jy$) |
|---|---|---|---|---|---|---|---|---|---|---|
| 4 | 8:54:18.771 | + 6:46:19.911 | 0.78 | 0.32 | 2.96 | 1.69 | 7.21 | 3.30 | 15.13 | 10.86 |
| 5 | 8:54:18.711 | + 6:46:19.227 | 0.70 | 0.67 | 1.36 | 1.12 | 2.33 | 1.57 | 2.98 | 1.43 |
| 6 | 8:54:18.795 | + 6:46:20.936 | 2.36 | 1.79 | 3.61 | 2.45 | 6.39 | 5.10 | 8.25 | 4.19 |
| 7 | 8:54:18.790 | + 6:46:21.158 | 4.55 | 3.26 | 6.85 | 4.58 | 11.12 | 6.82 | 14.47 | 8.17 |
| 8 | 8:54:18.794 | + 6:46:21.328 | 4.35 | 3.18 | 6.55 | 5.10 | 10.63 | 7.03 | 13.86 | 8.40 |
| G14-1 | | | | | | | | | | |
| 1 | 14:54:28.387 | +00:44:34.27 | 2.58 | 2.17 | 6.11 | 4.90 | 12.84 | 11.97 | 23.33 | 18.73 |
| 2 | 14:54:28.324 | +00:44:34.59 | 13.71 | 11.80 | 25.17 | 23.21 | 39.50 | 30.96 | 55.99 | 42.53 |
| 3 | 14:54:28.307 | +00:44:33.91 | 3.17 | 2.82 | 5.23 | 4.07 | 10.09 | 7.92 | 13.19 | 7.61 |

**Table A2.** Properties of clumps in DYNAMO galaxies.

| ID<br>D13-5 | $\log M_{\star,\,\mathrm{raw}}$ ($M_\odot$) | $\log M_{\star,\,\mathrm{discsub}}$ ($M_\odot$) | $Position_{\mathrm{clump}}/R_{\mathrm{gal,85\ per\ cent}}$ | Size (Kpc) |
|---|---|---|---|---|
| 1 | 7.14 | 6.90 | 0.53 | 0.25 |
| 2 | 7.48 | 7.32 | 0.72 | 0.34 |
| 3 | 7.68 | 7.20 | 0.37 | 0.29 |
| 4 | 7.21 | 7.13 | 0.34 | 0.27 |
| 5 | 7.92 | 6.95 | 0.34 | 0.55 |
| 6 | 7.75 | 7.37 | 0.34 | 0.46 |
| 7 | 7.34 | 7.21 | 0.40 | 0.24 |
| 8 | 8.03 | 7.44 | 0.27 | 0.39 |
| 9 | 7.95 | 7.63 | 0.34 | 0.39 |
| 10 | 7.76 | 6.39 | 0.35 | 0.43 |
| 11 | 7.94 | 7.77 | 0.34 | 0.44 |
| 12 | 7.23 | 6.00 | 0.46 | 0.19 |
| 13 | 7.78 | 7.80 | 0.34 | 0.32 |
| 14 | 7.59 | 7.02 | 0.89 | 0.25 |
| 15 | 6.94 | 6.58 | 0.83 | 0.28 |
| 16 | 7.75 | 5.65 | 0.95 | 0.50 |
| 17 | 6.87 | 6.37 | 1.17 | 0.22 |
| D15-3 | | | | |
| 1 | 7.52 | 7.06 | 0.47 | 0.28 |
| 2 | 7.17 | 6.80 | 0.68 | 0.24 |
| 3 | 6.67 | 5.47 | 0.47 | 0.15 |
| 4 | 7.35 | 6.82 | 0.48 | 0.26 |
| 5 | 7.71 | 7.20 | 0.29 | 0.28 |
| 6 | 7.21 | 7.14 | 0.35 | 0.21 |
| 7 | 7.57 | 7.41 | 0.18 | 0.22 |
| 8 | 8.11 | 7.68 | 0.13 | 0.34 |
| 9 | 7.43 | 6.78 | 0.36 | 0.25 |
| 10 | 7.62 | 7.88 | 0.28 | 0.34 |
| 11 | 7.33 | 7.11 | 0.35 | 0.28 |
| 12 | 7.48 | 7.01 | 0.45 | 0.26 |

**Table A2** – *continued*

| ID D13-5 | $\log M_{\star,\,\mathrm{raw}}$ ($M_\odot$) | $\log M_{\star,\,\mathrm{discsub}}$ ($M_\odot$) | $Position_{\mathrm{clump}}/R_{\mathrm{gal,85\ per\ cent}}$ | Size (Kpc) |
|---|---|---|---|---|
| G04-1 | | | | |
| 1 | 7.35 | 6.80 | 0.68 | 0.41 |
| 2 | 8.35 | 8.47 | 0.50 | 0.65 |
| 3 | 7.82 | 8.39 | 0.49 | 0.48 |
| 4 | 8.08 | 8.80 | 0.56 | 0.54 |
| 5 | 8.18 | 7.77 | 0.70 | 0.65 |
| 6 | 7.68 | 7.70 | 0.89 | 0.60 |
| 7 | 7.22 | 6.99 | 1.02 | 0.40 |
| 8 | 8.58 | 8.62 | 0.22 | 0.59 |
| 9 | 8.78 | 8.72 | 0.14 | 0.62 |
| 10 | 9.01 | 8.63 | 0.06 | 0.77 |
| 11 | 8.26 | 8.48 | 0.48 | 0.52 |
| 12 | 8.19 | 7.61 | 0.61 | 0.64 |
| 13 | 7.75 | 8.28 | 0.62 | 0.43 |
| 14 | 7.66 | 6.91 | 0.58 | 0.39 |
| G20-2 | | | | |
| 1 | 7.27 | 6.61 | 1.16 | 0.60 |
| 2 | 7.42 | 7.30 | 0.98 | 0.51 |
| 3 | 8.40 | 8.02 | 0.47 | 0.79 |
| 4 | 7.70 | 7.53 | 1.18 | 0.59 |
| 5 | 9.25 | 9.00 | 0.40 | 1.12 |
| 6 | 9.09 | 8.53 | 0.58 | 0.87 |
| 7 | 7.72 | 7.24 | 0.99 | 0.47 |
| 8 | 9.23 | 9.31 | 0.13 | 0.52 |
| 9 | 8.99 | 8.59 | 0.55 | 0.92 |
| 10 | 8.63 | 8.20 | 0.55 | 0.76 |
| 11 | 8.93 | 8.65 | 0.48 | 0.89 |
| 12 | 9.57 | 9.032 | 0.30 | 1.44 |
| G08-5 | | | | |
| 1 | 7.39 | 7.05 | 0.66 | 0.42 |
| 2 | 7.80 | 8.03 | 0.66 | 0.52 |
| 3 | 8.08 | 8.31 | 0.39 | 0.54 |
| 4 | 8.26 | 8.35 | 0.35 | 0.69 |
| 5 | 7.41 | 6.88 | 0.79 | 0.43 |
| 6 | 7.79 | 7.58 | 0.46 | 0.54 |
| 7 | 8.01 | 7.69 | 0.55 | 0.71 |
| 8 | 8.00 | 7.71 | 0.64 | 0.73 |
| G14-1 | | | | |
| 1 | 8.24 | 8.45 | 0.33 | 0.57 |
| 2 | 8.58 | 8.26 | 0.45 | 0.44 |
| 3 | 8.05 | 7.89 | 0.63 | 0.64 |

This paper has been typeset from a TEX/LATEX file prepared by the author.